Analysis of Third Order Dispersion in Ultra-High Speed Optical Fiber Communication System and Its Compensation Technique

By

Farzana Rahmat Zaki

A thesis submitted to the Department of Electrical and Electronic Engineering of Bangladesh University of Engineering and Technology in partial fulfillment of the requirement for the degree of

MASTER OF SCIENCE IN ELECTRICAL AND ELECTRONIC ENGINEERING

Department of Electrical and Electronic Engineering

BANGLADESH UNIVERSITY OF ENGINEERING AND TECHNOLOGY

February 2013

The thesis titled **"Analysis of Third Order Dispersion in Ultra-high Speed Optical Fiber Communication and Its Compensation Technique"** submitted by Farzana Rahmat Zaki, Student No:100706213P, Session: October, 2007, has been accepted as satisfactory in partial fulfillment of the requirement for the degree of MASTER OF SCIENCE IN ELECTRICAL AND ELECTRONIC ENGINEERING on February 23, 2013.

BOARD OF EXAMINERS

1.____________________ Chairman (Supervisor)

Dr. Mohammad Faisal
Assistant Professor
Department of Electrical and Electronic Engineering
Bangladesh University of Engineering and Technology (BUET)
Dhaka – 1000, Bangladesh

2.____________________ Member (Ex-officio)

Dr. Pran Kanai Saha
Professor and Head
Department of Electrical and Electronic Engineering
Bangladesh University of Engineering and Technology (BUET)
Dhaka – 1000, Bangladesh

3.____________________ Member

Dr. Md. Saiful Islam
Professor and Director
Institute of Information and Communication Technology
Bangladesh University of Engineering and Technology (BUET)
Dhaka – 1000, Bangladesh

4.___________________ Member (External)

Gp Capt Dr. Mohammed Hossam-E-Haider
Senior Instructor and Head
Department of Electrical, Electronic and Communication Engineering
Military Institute of Science and Technology
Mirpur Cantonment, Dhaka-1216, Bangladesh

CANDIDATE'S DECLARATION

It is hereby declared that this thesis or any part of it has not been submitted elsewhere for the award of any degree or diploma and that all sources are acknowledged.

Signature of the Candidate

____

Farzana Rahmat Zaki

DEDICATION

To my parents and husband.

ACKNOWLEDGEMENT

The author would like to express her sincere appreciations to Dr. Mohammad Faisal for his excellent supervising. This thesis would not have been completed without his support and guidance. I would like to express my great thanks and gratefulness for his instructions, continuous encouragement, valuable discussions, and careful review during the period of this research. His keen sight and a wealth of farsighted advice and supervision have always provided me the precise guiding frameworks of this research. I have learned many valuable lessons and concepts of optical fiber communication from him through my study, which I have utilized to develop my abilities to work innovatively and to boost my knowledge. His constant encouragement gave me the confidence to carry out my work. I am very much thankful to him for helping me by providing all the necessary information, discussions and proper guidance.

I would like to thank all my teachers. They gave the knowledge and directions that have helped me throughout my life. I express my gratitude to my teachers from Bangladesh University of Engineering and Technology. The knowledge I learned from the classes in my M.Sc. levels were essential for this thesis.

I would also like to thank the authority of the university (BUET) as it always provided me with necessary software and allow me to use the laboratory.

I am also thankful to my family and friends who supported me generously and encourage me enormously to complete this job.

Last but not the least; the author must convey her gratefulness towards almighty Allah. Without His mercy and help, it would not be possible to complete the job properly.

ABSTRACT

The introduction of WDM with optical amplifiers has revolutionized the optical fiber transmission system by escalating the system capability both by the number of channels and distance. Transmission capacity can be further improved by increasing the channel bit rate. The channel bit rate is upgraded to 40 Gb/s from 10 Gb/s and it is predicting that the next generation light wave communications will be based on 100 Gb/s rate or even more. This high bit rate systems will face many problems due to fiber dispersion and nonlinearity which are interconnected with transmitting power, number of channels, channel spacing, transmission length and duty cycle. The third order dispersion (TOD) effect still may be in an acceptable limit at current bit rate of optical fiber transmission scheme but its effect increases with the escalating bit rate. The presence of the TOD causes pulse broadening and ripples as well as introduces an additional temporal shift to each pulse. As a result compensation of third order dispersion along with second order dispersion has become a concern now-a-days in dispersion-managed system. This fact has motivated us in this research.

In this work a comprehensive investigation on pulse distortions has been carried out due to the TOD on ultra-high speed long-haul single channel optical fiber communication system. The optical communication system consists of dispersion-management with a periodic Er-doped fiber amplifier (EDFA). Impact of TOD is observed at the receiving end considering the variation of different factors such as bit rate, duty cycle, pulse shape, transmission distance and fiber type. Only self-phase modulation, second and TOD effects, fiber loss, ASE noise and receiver noises are considered here. In the simulation, two different dispersion-managed models have been used. One model consists of standard single mode fiber and dispersion compensated fiber (DCF). In another model, non-zero-dispersion shifted fiber is followed by DCF. Each span consists of an optical amplifier at the end terminal of every span. The numerical simulation is done by directly solving the Nonlinear Schrodinzer equation using split-step Fourier method. The simulation has been carried out using OptiSystem. Pulse center position changes with the variation of duty cycle, pulse shape and fiber type. However, these impairments could be mitigated by properly designing DM transmission systems along with consideration of other parameters. As far as real environment is considered, performance of SSMF-FBG is satisfactory while considering both GVD and TOD for high bit rate. The result obtained from this work will be helpful for designing high-speed long-haul optical fiber communication system.

CONTENTS

List of Figures

List of Tables

List of Symbols

B	Bit Rate
b	Number of Bits
L	Repeater Spacing
v_g	Group Velocity
τ_g	Group Delay
λ	Wavelength
β	Propagation Constant
V	Normalized Frequency
b	Normalized Propagation Constant
λ_0	Zero Dispersion Wavelength
Δ	Index Difference
P	Induced Polarization
E	Electric Field
n_2	Non-linear Refractive Index
T_0	Initial Width
P_0	Peak Power
L_D	Dispersion Length
L_{NL}	Nonlinear Length
β_2	GVD Parameter
β_3	TOD Parameter
γ	Nonlinear Parameter
T_r	Rise Time
T_B	Bit Slot
L_m	Dispersion-Map Period
Q	Quality Factor
S	Dispersion Slope
A_{eff}	Fiber Effective Area

List of Abbreviations

ATM	Asynchronous Transfer Mode
OFC	Optical Fiber Communication
WDM	Wavelength-Division Multiplexing
FSK	Frequency Shift Keying
PSK	Phase Shift Keying
SNR	Signal to Noise Ratio
BER	Bit Error Rate
SM	Single mode
ZMD	Zero Material Dispersion
SPM	Self-Phase Modulation
XPM	Cross- Phase Modulation
SRS	Stimulated Raman Scattering
SBS	Stimulated Brillouin Scattering
TOD	Third Order Dispersion
DS	Dispersion Slope
DM	Dispersion Managed
DCF	Dispersion Compensated Fiber
FBG	Fiber Bragg Grating
GVD	Group Velocity Dispersion
SSMF	Standard Single Mode Fiber
DSF	Dispersion Shifted Fiber
NZDSF	Non-zero Dispersion Shifted Fiber
NLS	Nonlinear Schrodinger
FWHM	Full Width Half Maximum
LED	Light-Emitting Diode
FFT	Finite-Fourier-Transform
PRBS	Pseudo-Random Binary Sequence
GUI	Graphical User Interface

NRZ	Non-Return-to-Zero
RZ	Return-to-Zero
CW	Continuous Wave
MZ	Mach-Zehnder
SF	Symmetry Factor
SOA	Semiconductor Optical Amplifier
EDFA	Erbium-Doped Fiber Amplifier
ASE	Amplified Spontaneous Emission
OTDV	Optical Time Domain Visualizer
FROG	Frequency Resolved Optical Gating
OSA	Optical Spectrum Analyzer

Chapter One

Introduction

1.1 Introduction

In the last few years, there has been vast increase of applications in telecommunications sectors that require great amounts of bandwidth such as interactive multimedia, video conferencing and streaming audio made the capacity of the exiting optical fiber systems inadequate. Technologies such as Frame Relay and ATM also require capacity increase. Internet users are increasing by 700 percent each year which in turn is also becoming threatening to telephone access networks [1]. As a result, service providers must ensure fault-tolerant services. During the past several years, different steps and market-driven economic policies have been initiated to promote the telecommunication sector throughout the world. But today's competitive advantage focuses on escalating the existing capacity of network infrastructures and providing improved consistency [2].

To fulfill these requirements, carriers have broadened route diversity, through ring configurations in which back-up capacity is provided on alternate fibers. Achieving 100% reliability however requires that spare capacity be set aside. This potentially doubles the bandwidth need of an already strained and overloaded system. Growth of cellular is also placing more demand on fiber networks. At the same time carriers are enhancing network survivability, they must also accommodate growing customer demand for services such as video, high resolution graphics and large volume data processing that require large amounts of bandwidth [2]. Thus the deployment of future optical networks and upgrade of existing ones will be governed by the growth of the traffic in all network areas.

1.2 Recent Advancements in Optical Fiber Communications

The development of optical communications has made steadfast advancement since the invention of fiber optics. Over the years, fiber optics has formed the backbone of modern information technology. With the increasing dominance of smart mobile devices and bandwidth-hungry applications such as cloud computing, YouTube, Facebook and other social network activities, the overall speed demand are increasing at an outstanding rate and major telecommunication service providers are incessantly looking for technological breakthroughs that could further push the network speed limits. While the transportation of the data bits between different points in such networks normally makes use of light pulses, it is quite a different story for the switching and routing of the data at the network nodes. Due to the absence of good optical random access memories, up to now, the data needed to be converted from the optical to the electrical domain and electronic switches with microelectronic processors were needed. However, with the ever increasing amount of data the power consumption of such optoelectronic switches increases dramatically.

Several experiments have demonstrated signal transmission over distances 100 km at high bit rates (100 Gb/s or more) using simultaneous compensation of both GVD and TOD. In a 1996 experiment, a 100-Gb/s signal was transmitted over 560 km with 80-km amplifier spacing [3]. In a later experiment, bit rate was extended to 400 Gb/s by using 0.98-ps optical pulses within the 2.5-ps time slot [4]. Without compensation of the TOD, the pulse broadened to 2.3 ps after 40 km and exhibited a long oscillatory tail extending over 5–6 ps. With partial compensation of TOD, the oscillatory tail disappeared and the pulse width reduced to 1.6 ps. In another experiment [5], a planar lightwave circuit was designed to have a dispersion slope of 15:8 ps/nm2 over a 170-GHz bandwidth. It was used to compensate the TOD over 300 km of a dispersion-shifted fiber. The dispersion compensator eliminated the long oscillatory tail and reduced the width of the main peak from 4.6 to 3.8 ps.

In a later experiment, a liquid-crystal modulator was used to compensate for the residual β_3 [6], and the pulse remained nearly unchanged after propagating over 2.5 km of the dispersion-compensated fiber link. In a 1999 experiment [7], the use of the same technique with a different DCF (length 1.5 km) permitted transmission of a 0.4-ps pulse over 10.6 km of fiber with little distortion in the pulse shape.

1.3 Background of the study

With the rapid growth of the information industry throughout the world, more attention is being given to fiber optic communication networks having high speed and larger capacity. Dispersion greatly hampers the performance of optical fiber communication. It also degrades system performance due to increase inter chip interference and reduced received optical power [8, 9]. So if dispersion can be minimized then a further performance can be obtained from optical fiber communication.

Dynamic dispersion compensation is becoming paramount in high-speed wavelength-division multiplexed (WDM) light wave systems, operating at 40 Gb/s and beyond as the expansion of the transmission bandwidth has led to the signal waveform distortion. Even if the transmission bandwidth is limited to a single channel, third order dispersion (TOD) causes pulses to have trailing ripples in ultrahigh speed optical transmission systems [10-12]. Hence, in such a high bit rate systems, it becomes increasingly important to exactly compensate not only the second-order, but also the TOD or dispersion slope (DS) of the fiber as they impose a high dispersion penalty. Therefore a device, capable of tunability of the dispersion slope is highly desirable to dynamically match an arbitrary amount of accumulated dispersion slope.

To reduce the effect of dispersion, many fiber structures such DSF, NZDSF have been proposed. But this kind of fiber is not efficient in a WDM system due to the nonlinear effect. There have been several proposals to compensate for fiber dispersion effects. These include alternating fibers with positive and negative dispersion, electronic equalization in the IF-band for coherent systems, and compensation with laser chirp, etc [13-16]. Among the different dispersion compensation techniques, there are two methods that are very useful, one using the dispersion compensation fiber (DCF), the other using optical fiber Bragg grating (FBG). But dispersion slope of DCF does not completely match those of G.652 and G.655 fibers. FBG, however, is very compatible with most of the present optical fiber communication systems and has wide application foreground [10-19]. However, all these analyses use bit rate of 10 Gb/s and/or 40 Gb/s over single channel or WDM system. Also, most of the system did not use real value. These analyses investigated the TOD effect neglecting group velocity dispersion (GVD) parameter which is not practical for standard single mode fiber (SSMF) transmission system [20-21]. So, an optimum model for ultra-high speed system is essential for better fiber-optic communication. Therefore, in the present thesis, we shall examine the pulse shape and the temporal effect for ultra-high speed system considering GVD parameter without TOD and with TOD and evaluate the impact on transmission system. Then we will model a dispersion compensation system which will be beneficial for designing the ultra-high speed optical fiber communication system

1.4 Objectives

The objectives of this thesis are:

i. To investigate the TOD effect for different high bit rate systems (40 Gb/s, 100 Gb/s and 160 Gb/s) for single type fiber (SSMF, DSF, NZDSF).

ii. To explore the TOD effect for different high bit rate systems (40 Gb/s, 100 Gb/s and 160 Gb/s), duty cycle and dispersion map strength for dispersion managed (DM) transmission systems. Two different models will be studied. One model consists of SSMF and DCF. In another model, NZDSF is followed by DCF. We will also check the time-shift without and with TOD.

iii. To evaluate the TOD compensation using FBG for ultra-high speed optical communication system.

1.5 Thesis Outline

Chapter one covers the introduction, recent advancements, background and objectives of the present thesis.

Chapter two represents the impact of different transmission impairments of optical fiber communication system.

In chapter three, the basic theories for the analyses employed in this thesis for DM transmission will be presented. Fundamental equations of optical pulse propagation in a fiber have been studied. Analytical calculation of pulse broadening and changes of pulse shapes due to GVD and TOD on RZ Gaussian pulse will be explained. For checking the results of analytic techniques, we have introduced a numerical technique known as Split Step Fourier Method (SSFM).The dispersion managed system is also focused in this chapter.

The simulation model using OptiSystem will be represented in chapter four. Dispersion compensated system model has three parts- transmission section, optical link section and receiver section. Components of the each section will be also discussed in this chapter.

Simulation results are discussed in chapter five. Two different models are used to explore the TOD effect for different high bit rate systems, duty cycle, dispersion map strength and fiber types for dispersion managed transmission system. One model consists of SSMF and DCF. In another model, NZDSF is followed by DCF. We will also check the time-shift without and with TOD. We will also use the TOD compensation technique using fiber Bragg's grating for ultra-high speed optical communication system.

Chapter six is the concluding chapter. It contains the summary of the work. The chapter also highlights scopes for future work. All references are placed at the end of this thesis.

Chapter Two

Transmission Impairments of Optical Fiber

2.1 Introduction

The ultimate goal of the optical signal transmission is to achieve the predetermined bit-error ratio (BER) between any two nodes in an optical network. The optical transmission system has to be properly designed in order to provide the reliable operation during its lifetime. However, as data rates in optical networks increases, it is needed to pay more attention to peculiarities in the fiber-optic medium. High bit rate systems face many problems due to fiber dispersion and nonlinearity which are interrelated with transmitting power, number of channels, channel spacing ,bit rate and transmission length, etc.

In this chapter, we will discuss the basic transmission impairments in optical fiber communication in section 2.2. Sub-section 2.2.1 presents a brief discussion on linear impairments. Non linear impairments are presented in sub-section 2.2.2.

2.2 Impairments of Optical Fiber Communication

The transmission impairments of optical fiber can be classified into two main effects: linear and nonlinear. Linear effects include fiber attenuation and dispersion, and nonlinear effect consists of inter-channel and intra-channel impairments.

2.2.1 Linear Impairments

In optical fiber communication systems, linear impairments are due to the fiber loss and chromatic dispersion (CD). Different linear effects are briefly describer below-

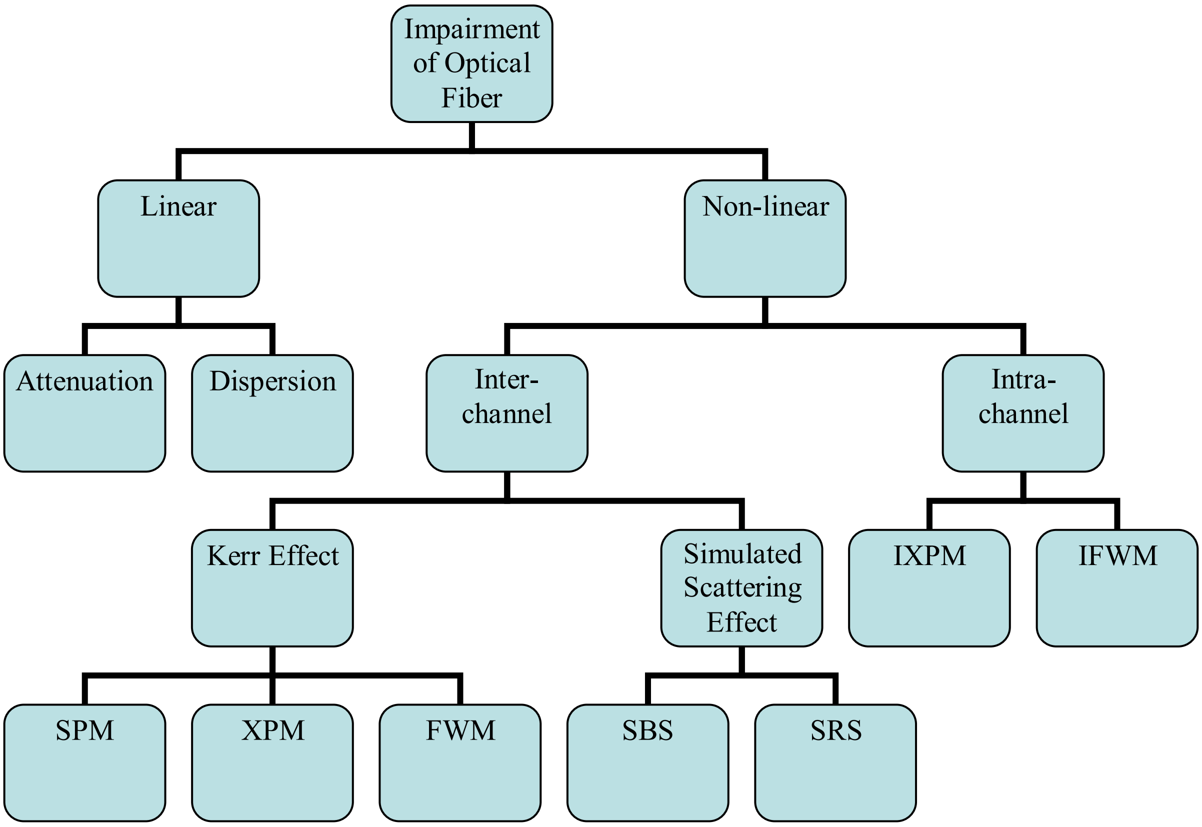

Figure 2.1: Transmission impairments of optical fiber.

2.2.1.1 Attenuation

Once power is coupled into the fiber, the optical signal will interact with the fiber. One of these interactions is the attenuation or loss of the light signal as it moves through the medium. Signal attenuation is defined as the optical output power P_{out} from a fiber of length L to the optical input power P_{in}. Mathematically

$$P_{out} = P_{in} \exp(-\alpha L) \qquad (2.1)$$

Where α is attenuation constant account to fiber loss. Usually, fiber loss is expressed in terms of dB/km where $\alpha_{dB} = 4.343\alpha$. Although power of the pulse is attenuated due to fiber loss, full width at half maximum (FWHM) of the pulse remains unchanged.

The loss of power depends on the wavelength of the light and on the propagating material. For silica glass, the shorter wavelengths are attenuated the most. Attenuation is caused by two physical effects, which are absorption and scattering. Absorption has an effect of removing photons, when they interact with atoms and molecules of the medium while scattering redirects the light out of the core of the fiber.

Scattering losses occur when the photons see a variation in the core's refractive index. This phenomenon is Raleigh scattering and is considered as an intrinsic loss in optical fiber and therefore sets the lower limit on fiber losses. Thus attenuation in optical fiber is obtained by considering effects of absorption and scattering simultaneously. The lowest attenuation occurs at wavelengths 1300 nm and 1550 nm with the corresponding values of 0.5 dB/km and 0.2 dB/km, respectively. The 1550 nm window is favored in telecommunication applications considering the theoretically minimum for fused silica fiber.

2.2.1.2 Fiber Dispersion

Ideally, an optical pulse with a given FWHM and amplitude, transmitted into one end of a fiber should arrive at the far end of that fiber with its shape unchanged; however the optical pulse not only loses its power but the pulse broadens as it propagates. The phenomenon of broadening of a pulse during its propagation through the optical fiber is known as dispersion. The widened pulse may merge into its neighboring pulses and cause transmission errors. The dispersion phenomenon is illustrated in fig. 2.2.

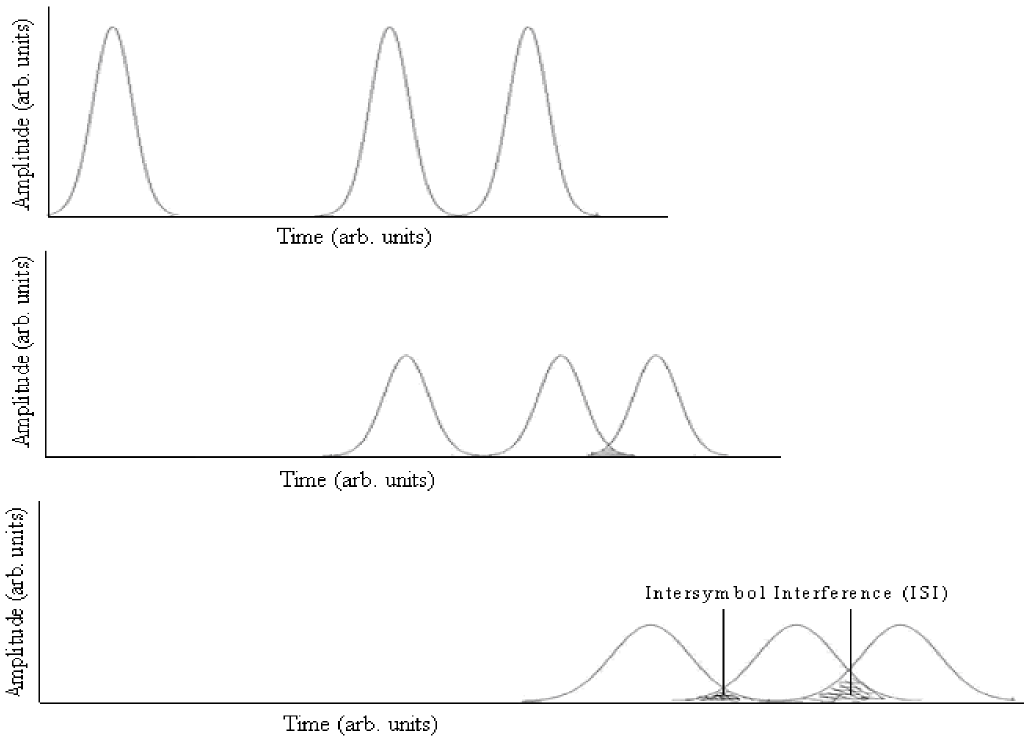

Figure 2.2: Pulse broadening due to dispersion and illustration of ISI (a) Pulses at the input of the fiber, (b) fiber output at distance z_1, (c) fiber output at distances $z_2 > z_1$.

The figure shows that each pulse broadens and overlaps with its neighboring pulses. Due to overlapping, the propagating pulses eventually may become impossible to differentiate at the receiver input. This effect is known as “Inter Symbol Interference” (ISI). Thus, an increasing number of errors may be encountered on the digital optical channel as the ISI becomes more prominent. The pulses can be separated by spacing them out at the transmitter, but this means reducing the transmission bit rate. Hence, fiber transmission distance is limited due to both of the fiber loss and dispersion.

Dispersion in optical fibers occurs due to dependence of the propagation phase constant and the refractive index of the core material on the transmitted wavelengths. The different wavelengths propagate at different velocities and results in dispersion of the output pulse shape in time.

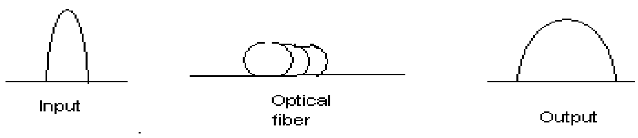

Figure 2.3: Dispersion in fiber.

In multi-mode fibers, dispersion is also caused by the different propagation time for the different modes which is called modal or inter-modal dispersion. Dispersion in optical fibers can be classified into two major types: (i) Intramodal dispersion (ii) Inter-modal dispersion. Intramodal dispersion: Intramodal dispersion is of types viz. (i) Material dispersion (ii) Waveguide dispersion.

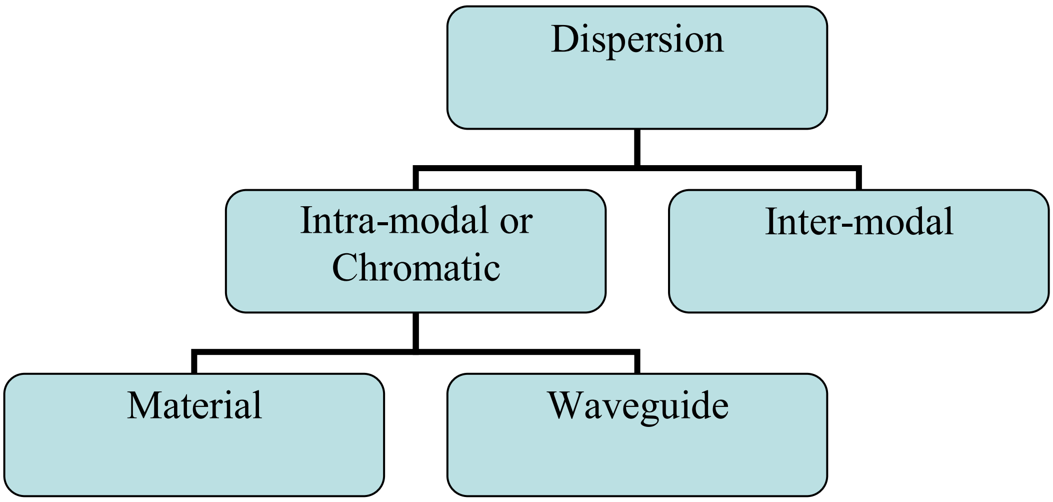

Figure 2.4: Different types of dispersion.

In multimode fiber, the incident light can take many different paths or ‘modes’ as it propagates through the fiber. Each mode traverses a unique path along the fiber to reach output and therefore arrives at a different time resulting in pulse spreading. This category of dispersion, called modal dispersion, only applies to multimode fibers.

Single mode fiber (SMF) is used to avoid modal dispersion. Only the fundamental mode propagates in SMF hence no modal dispersion is experienced by the propagating signal. However in SMF, chromatic dispersion is the dominant phenomenon discussed below.

Chromatic Dispersion:

Intramodal or chromatic dispersion may occur in all types of optical fibers and results from finite spectral width of the optical source. The different emitted wavelengths of the optical source will travel at different group velocities due to different refractive index for different wavelengths as $d^2n/d\lambda^2 \neq 0$. As a result, the different wavelengths arrive at the destination at different times. The variation of refractive index with wavelength is dependent on the glass material and so this form of dispersion is called material dispersion. In digital transmission (digital modulation of the optical carrier), dispersion results in smearing of the optical pulses and thus affects the maximum data rate of transmission.

Waveguide dispersion results from variation of group velocity with wavelength. This is due to variation of the incident angle with wavelength which consequently leads to a variation in the transmission times for the rays with different incident angles. For a SM fiber whose propagation constant is β, the fiber exhibits waveguide dispersion when $d^2\beta/d\lambda^2 \neq 0$. In SM fibers, waveguide dispersion may be comparable with material dispersion.

Fiber dispersion plays important role in pulse propagation because different spectral components travel at different speeds, represented as c/n(ω), where c is the velocity of light and n(ω) is frequency dependent refractive index of the fiber. Mathematically, the effects of fiber dispersion are studied by expanding mode propagation constant β(ω) in Taylor series around the frequency ω_0 as

$$\beta(\omega) = n(\omega)\frac{\omega}{c} = \beta_0 + \beta_1(\omega-\omega_0) + \frac{1}{2}\beta_2(\omega-\omega_0)^2 + \ldots\ldots\ldots \tag{2.2}$$

where n is the core refractive index, ω0 is the central frequency of the pulse spectrum and

$$\beta_m = \left(\frac{d^m\beta}{d\omega^m}\right)_{\omega=\omega_0} \quad (m = 1, 2, \ldots\ldots) \tag{2.3}$$

Using equations (2.2) and (2.3), the expression for β_1 can be derived as

$$\beta_1 = \frac{d\beta}{d\omega} = \frac{1}{c}(n + \omega\frac{dn}{d\omega}) \tag{2.4}$$

As by definition, β_1 is inverse of the group velocity v_g, hence equation (2.4) can be represented as

$$\beta_1 = \frac{1}{v_g} = \frac{1}{c}(n + \omega\frac{dn}{d\omega}) = \frac{n_g}{c} \tag{2.5}$$

where n_g is the group index. Similarly, using equations (2.3) and (2.5), the expression for β_2, named as GVD parameter, will be

$$\beta_2 = \frac{d\beta_1}{d\omega} = \frac{1}{c}(2\frac{dn}{d\omega} + \omega\frac{d^2n}{d\omega^2}) \tag{2.6}$$

The mathematical relations (2.5) and (2.6) can be explained physically that the optical pulse moves at the group velocity while the group velocity dispersion is represented by β_2 that causes pulse broadening.

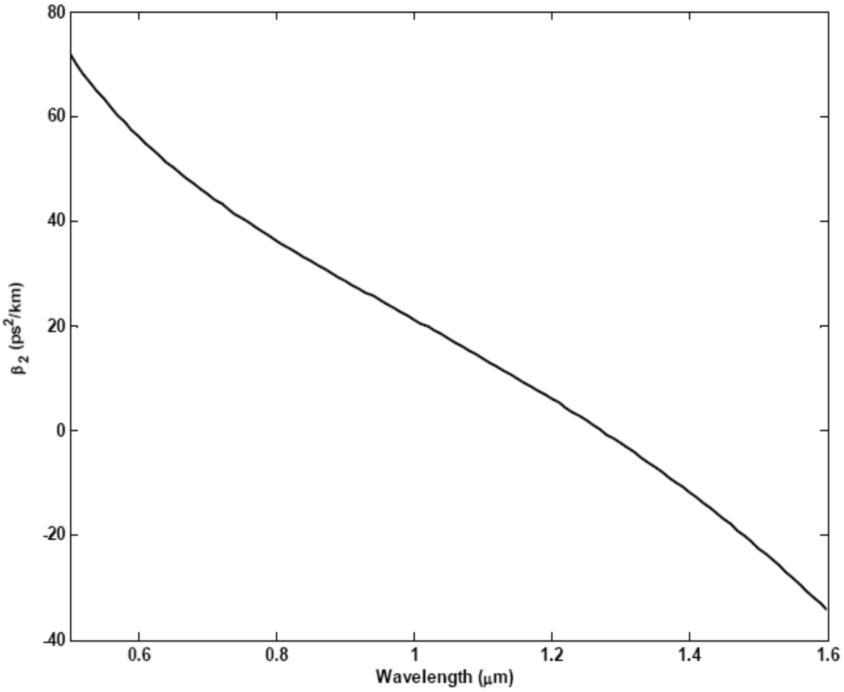

Figure 2.5: Variation of β_2 with wavelength for fused silica.

It is clear from fig. 2.5 that for the wavelength of 1.27 μm, denoted as λ_d, the effect of β_2 vanishes. The values of β_2 are positive for wavelengths less than λ_d, while they become negative for wavelengths greater than λ_d. The region for $\beta_2 > 0$ is called normal dispersion regime while the region for $\beta_2 < 0$ is known as anomalous dispersion regime.

The pulse degradation effect due to GVD parameter β_2 and TOD parameter β_3 will be discussed in detail in the next chapter.

2.2.2 Nonlinear Impairments

Most nonlinear effects arise due to intensity dependent refractive index of the fiber. When an electromagnetic field interacts with the atoms and molecules of the fiber, it induces an oscillating polarization which causes a tiny change in the refractive index of the fiber. It is called Kerr effect. For low intensities, the polarization behaves linearly to the applied field; therefore perturbation of the field can be characterized by a constant refractive index. However the effect is nonlinear at high intensities and Kerr nonlinearities may be observed. Due to Kerr effect, different points within a single Gaussian pulse of light (as they have different intensities) experience different refractive indices in the fiber that causes an intensity dependent phase shift. This phenomenon is called self-phase modulation (SPM). SPM basically introduces chirp in the propagating pulse that causes spectral broadening of the pulse.

If the incident light has lower intensity then the response of the medium is linear and governed by the equation

$$P = \varepsilon_0 \chi^{(1)} . E \tag{2.7}$$

However for higher intensities, the nonlinear effects cannot be neglected and the induced polarization is given by the equation

$$P = \varepsilon_0 (\chi^{(1)} . E + \chi^{(2)} : EE + \chi^{(3)} : EEE + ...) \tag{2.8}$$

where the polarization P has both linear and nonlinear components due to the applied electric field E, ε_0 is the vacuum permittivity, and $\chi^{(j)}$ is j^{th} order susceptibility. The linear susceptibility $\chi^{(1)}$ results in dominant contribution to P. Second order susceptibility $\chi^{(2)}$ in silica fibers vanishes since the SiO_2 molecules are symmetric. The lowest-order nonlinear effects in optical fiber arise due to third order susceptibility $\chi^{(3)}$. Nonlinear refraction, a phenomenon that refers to intensity dependent refractive index, is responsible for most of the nonlinear effects in optical fiber. The refractive index can be represented mathematically as

$$\tilde{n}(\omega, |E|^2) = n(\omega) + n_2 |E|^2 \tag{2.9}$$

where $n(\omega)$ is linear part of the refractive index that can be approximated by Sellmeier equation, $|E|^2$ represents optical intensity inside the fiber, the term n_2 is nonlinear index coefficient which is related to third order susceptibility as

$$n_2 = \frac{3}{8n} \mathrm{Re}(\chi^{(3)}_{xxxx}) \tag{2.10}$$

where Re means the real part, and $\chi^{(3)}_{xxxx}$ is the fourth-rank tensor. It is assumed that optical field is linearly polarized, and therefore only one component of $\chi^{(3)}$ contributes to the refractive index.

There are many nonlinear effects which occur in single channel / multi-channel fiber optic links. In single channel, self-phase modulation is the most dominant nonlinear phenomenon. In multi-channel propagation, two or more optical fields having different wavelengths propagate simultaneously inside a fiber and interact with each other through the fiber nonlinearity while generating new waves in certain cases. Some important nonlinear effects are cross phase modulation (XPM), stimulated Raman scattering (SRS), stimulated Brillouin scattering (SBS), four-wave mixing (FWM) etc. These effects are briefly discussed in the following.

Self-Phase Modulation (SPM):

Self-phase modulation arises due to intensity dependence of refractive index. Due to SPM, an optical field propagating through fiber, experiences a self-induced intensity dependant nonlinear phase shift which leads to change in the frequency spectrum of the pulse. In this way, an initially un-chirped optical pulse acquires chirp i.e. a temporally varying instantaneous frequency.

Cross-Phase Modulation (XPM):

Cross-phase modulation refers to the change in the optical phase of a light beam in a nonlinear medium induced by another optical field propagating at a different wavelength, direction, or state of polarization. It arises due to the fact that the effective refractive index experienced by an optical field depends not only on the intensity of that beam but on the overall power contributing from co-propagating beams. XPM leads to asymmetric spectral broadening, intensity fluctuations and distortion of co-propagating optical pulses, thereby causing channel cross-talk.

Stimulated Raman Scattering (SRS):

Stimulated inelastic scattering, nonlinear in nature, is a phenomenon in which scattering of incident photon interacting with dielectric medium results in lower energy photon. The energy difference in this process is released in the form of phonons. The incident wave and the scattered wave are called ‘pump wave’ and ‘Stokes wave’, respectively. The result of stimulated inelastic scattering is loss of the incident energy.

Signals in optical fibers encounter two major types of stimulated inelastic scattering namely, stimulated Raman scattering and stimulated Brillouin scattering. The first is known as stimulated Raman scattering (SRS). This results when the energy transferred causes molecular vibration, which in turn modulates the incident light and generates new optical frequencies. Furthermore, the molecular vibration also provides optical amplification to newly generated frequencies. This is known as Raman gain.

Stimulated Brillouin Scattering (SBS):

The second effect is termed stimulated Brillouin scattering (SBS). SBS results when the vibrations generate an acoustic wave that travels in the same direction as the incident optical signal. The acoustic wave acts as a Bragg grating that reflects the light in the opposite direction. As it is moving, the Doppler shift gives rise to a frequency shift in the Scattered-light.

Four Wave Mixing (FWM):

When three EM waves with carrier frequencies ω_1, ω_2, and ω_3 (ω_1 and ω_2 may be equal, but ω_3 has to be distinct from both ω_1 and ω_2) co-propagate inside the fiber simultaneously, they generate a fourth EM wave whose frequency (ω_4) does not coincide with any of the three frequencies and is related to them by a relation $\omega_4 = \omega_1 \pm \omega_2 \pm \omega_3$. This phenomenon is referred as four wave mixing (FWM). In principle, generation of several frequencies is possible corresponding to different plus and minus sign combinations. However FWM is a phase-sensitive process which means that the interaction among different fields depends on their relative phases. The phase matching requirement restricts most of the combinations to build up. Frequency combinations of the form $\omega_4 = \omega_1 + \omega_2 - \omega_3$ often cause cross-talk or power imbalance between different wavelengths in multi-channel communication systems since they can become nearly phase-matched when channel wavelengths lie close to the zero-dispersion wavelength.

Four wave mixing can be reduced by spacing the channels unevenly as well as by increasing the channel spacing, reducing the transmitted power and increasing the operating wavelength. Though FWM is undesired in optical communications; it can be used for phase conjugation, holographic imaging, and optical image processing etc.

2.3 Conclusion

This chapter briefly discusses about two different types of transmission impairments of optical fiber. Linear barriers include fiber loss and dispersion, on the other hand nonlinear part comprises inter-channel and intra-channel impairments. Dispersion plays an important role in signal transmission over fibers. The interaction between dispersion and nonlinearity is an important issue in optical fiber system design.

Chapter Three

Theoretical Analysis of Dispersion in Optical Fiber Communication

3.1 Introduction

Chromatic dispersion or group velocity dispersion (GVD) is primarily the cause of performance limitation in the long haul optical fiber communication systems. Dispersion is the spreading out of a light pulse in time as it propagates down the fiber. As a result short pulses broaden, which leads to significant inter-symbol interference (lSI), and therefore, severely degrades the performance. Single mode fibers effectively eliminate inter-modal dispersion by limiting the number of modes to just one through a much smaller core diameter. However, the pulse broadening still occurs in SMFs due to intra-modal dispersion.

This chapter contains mathematical analysis of the effects of GVD and third-order dispersion (TOD) on a Gaussian and super-Gaussian pulse propagating through a single mode optical fiber. This work presents more detailed understanding of GVD and TOD effects on the propagating pulse and provides an opportunity to compare the results obtained from the numerical model with some well-known results available in the literature.

3.2 Pulse Propagation Model in Optical Fiber

The optical fiber component simulates the propagation of an optical field in a single-mode fiber with the dispersive and nonlinear effects taken into account by a direct numerical integration of the modified nonlinear Schrödinger (NLS) equation and a system of two, coupled NLS equations when the polarization state of the signal is arbitrary. The optical sampled signals reside in a single frequency band, hence the name total field. When the optical field is assumed to maintain its polarization along the fiber length, the evolution of a slowly varying electric field envelope can be described by a single nonlinear Schrödinger (NLS) equation of the form:

$$\frac{\partial E}{\partial z}+\alpha E+i\beta_2(\omega_0)\frac{\partial^2 E}{\partial T^2}-\frac{\beta_3(\omega_0)}{6}\frac{\partial^3 E}{\partial T^3}=i\gamma(|E^2|E+\frac{i}{\omega_0}\frac{\partial}{\partial T}(|E^2|E)-\rho\tau_{R1}E\frac{\partial |E|^2}{\partial T^2}) \tag{3.1}$$

In Equation 3.1, E = E (z, T) is the electric field envelope. A frame moving at the group velocity ($T = t - z/v_g = t - z\beta_1$) is assumed. The derivatives of the propagation constant of the fiber mode $\beta(\omega)$, $(\beta(\omega)c)/\omega)$, is the mode effective index), with respect to frequency

$$\beta_n=\frac{\partial^n\beta(\omega_0)}{\partial\omega^n}, n=1,2,3 \tag{3.2}$$

β_2 and β_3 are the first and the second GVD parameters, respectively, and ω_0 is the reference frequency of the signal, $\omega_0 = 2\pi c/\lambda_0$ with c being the light speed in vacuum.

The physical meaning of the terms in Equation (3.1) is the following. The first term takes into account the slow changes of the electric field along the fiber length. The second term takes into account the linear losses of optical fiber. The third term represents the (first-order) group velocity dispersion. This is the effect responsible for the pulse broadening. The next term is the second-order GVD, known also as TOD. This effect becomes important for a signal with a broad spectrum. The parameters β_2 and β_3 are denoted as "frequency domain parameters" in the interface of the component. The following relations are used internally to convert between them and the commonly used wavelength domain parameters D (dispersion) and S (dispersion slope).

$$D=\frac{d\beta_1}{d\lambda}=-\frac{2\pi c}{\lambda^2}\beta_2$$
$$\beta_3=(\frac{\lambda}{2\pi c})^2(\lambda^2 S+2\lambda D), S=\frac{dD}{d\lambda} \tag{3.3}$$

The parameter γ is given by:

$$\gamma=\frac{\omega_0 n_2}{cA_{eff}} \tag{3.4}$$

In Equation 3.4, n_2 is the nonlinear refractive index coefficient and A_{eff} is the fiber effective area. The first term in the right-hand side in Equation 3.1 accounts for the self-phase modulation effect. It is responsible for the broadening of the pulse spectra and, in the presence of anomalous GVD, for the formation of optical pulses. The second term in the right-hand side of Equation 3.1 takes into account the self-steepening effect. It leads to an asymmetry in the SPM-broadened spectra of ultra-short (femtosecond) pulses [9] and is responsible for the formation of optical shocks. The last term in Equation 3.1 accounts for the intra-pulse Raman scattering effect with the parameter τ_R being the parallel Raman self- shift time. The parameter ρ is the fractional contribution of the delayed response of the material to the total nonlinearity.

In dimensionless form, Equation 3.1 reduces to:

$$i\frac{\partial U}{\partial \xi}+D_2\frac{\partial^2 U}{\partial t^2}+N_1|U|^2U=iD_3\frac{\partial^3 U}{\partial t^3}+N_2U\frac{\partial |U|^2}{\partial t^2}-iN_3\frac{\partial}{\partial t}(|U|^2U)-iAU \tag{3.5}$$

where the coefficients are given by:

$$D_2=\frac{sign(\beta_2)}{2},D_3=\frac{L_D sign(\beta_3)}{L_D^{'}},N_1=\frac{L_D}{L_{NL}},N_2=\frac{L_D}{L_{NL}}\tau_R^{'},N_3=\frac{L_D}{L_{NL}}s \tag{3.6}$$

The new quantities are introduced according to:

$$L_D=\frac{T_0^2}{|\beta_2|},L_{NL}=\frac{1}{\gamma P_0},L_D^{'}=\frac{T_0^3}{|\beta_3|},s=\frac{1}{\omega_0 T_0},\tau_R^{'}=\frac{\tau_R}{T_0},E=\sqrt{P_0}U,T=T_0t,z=\zeta L_D \tag{3.7}$$

where U is the slowly varying amplitude of the pulse envelope and T is measured in a frame of reference moving with the pulse at the group velocity, initial width T_0 and the peak power P_0, GVD length L_D , the nonlinear length L_{NL} and $L_D^{'}$ as TOD length.

3.3 Effect of Second and Third Order Dispersions

In this thesis, we have considered the effect of GVD and TOD on ultra-high speed long-haul single channel optical fiber communication system. Suppose, incident power is 1mW. Therefore, neglecting fiber losses and nonlinear effects equation 3.5 reduces to

$$i\frac{\partial U}{\partial \xi}+D_2\frac{\partial^2 U}{\partial t^2}=iD_3\frac{\partial^3 U}{\partial t^3} \tag{3.8}$$

Equation (3.8) can be solved by using the Fourier-transform method. If $\tilde{U}$ (z,ω) is the Fourier transform of $U(z,T)$ such that

$$U(z,T) = \frac{1}{2\pi}\int_{-\infty}^{\infty} \tilde{U}(z,\omega)\exp(-i\omega T)d\omega \tag{3.9}$$

where

$$\tilde{U}(z,\omega) = \tilde{U}(0,\omega)\exp(\frac{1}{2}\beta_2\omega^2 z + \frac{1}{6}\beta_3\omega^3 z) \tag{3.10}$$

Equation (3.10) shows that both GVD and TOD change the phase of each spectral component of the pulse by an amount that depends on both the frequency and the propagated distance. Even though such phase changes do not affect the pulse spectrum, they can modify the pulse shape. By substituting equation (3.10) in equation (3.9), the general solution of equation (3.8) is given by

$$U(z,T) = \frac{1}{2\pi}\int_{-\infty}^{\infty} \tilde{U}(0,\omega)\exp(\frac{i}{2}\beta_2\omega^2 z + \frac{i}{6}\beta_3\omega^3 z - i\omega T)d\omega$$

(3.11)

where Ũ((0,ω) is the Fourier transform of the incident field at z= 0 and is obtained using

$$\tilde{U}(0,\omega) = \int_{-\infty}^{\infty} U(0,T)\exp(i\omega T)dT \tag{3.12}$$

Equations (3.11) and (3.12) can be used for different input pulses of arbitrary shapes.

3.3.1 Pulse Broadening Due to GVD for Gaussian Pulses

Consider the case of a Gaussian pulse for which the incident field is of the form [24]

$$U(0,T) = \exp(-\frac{T^2}{2T_0^2}) \tag{3.13}$$

where T_0 is the half-width. Usually, the full width at half maximum (FWHM) is used instead of T_0. For a Gaussian pulse, these two terms are related as

$$T_{FWHM} = 2T_0\sqrt{\ln(2)} \approx 1.665T_0 \tag{3.14}$$

By using Eqs. (3.13)–(3.14) and carrying out the integration, the amplitude at any point z along the fiber is given by

$$U(z,T) = \frac{T_0}{(T_0^2 - i\beta_2 z)^{\frac{1}{2}}}\exp(-\frac{T^2}{2(T_0^2 - i\beta_2 z)}) \tag{3.15}$$

Thus, a Gaussian pulse maintains its shape on propagation but its width T_1 increases with z as

$$T_1(z) = T_0[1+(\frac{z}{L_D})^2]^{\frac{1}{2}} \tag{3.16}$$

where the dispersion length $L_D = T_0^2 /|\beta_2|$. Equation (3.16) shows how GVD broadens a Gaussian pulse. The extent of broadening is governed by the dispersion length L_D. For a given fiber length, short pulses broaden more because of a smaller dispersion length. At $z = L_D$, a Gaussian pulse broadens by a factor of √2. Fig. 3.1 shows the extent of dispersion-induced broadening for Gaussian pulses by plotting $|U(z;T)|^2$ at $z = 2L_D$, and $4L_D$.

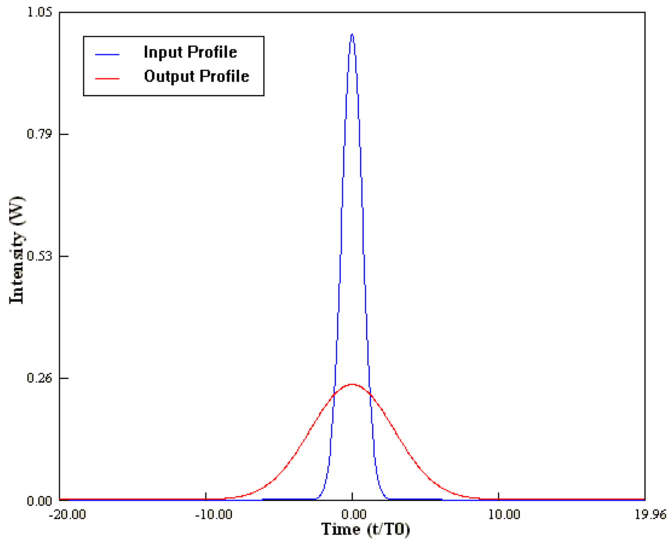

Figure 3.1: Dispersion-induced broadening of a Gaussian pulse inside a fiber at z = 2 L_D and z = 4L_D. Here, only β_2 is considered.

Although the incident pulse is unchirped (with no phase modulation), the transmitted pulse becomes chirped. This can be seen clearly by writing $U(z,T)$ in the form

$$U(z,T) = |U(z,T)| \exp[i\phi(z,T)] \tag{3.17}$$

where $$\phi(z,T) = -\frac{\mathrm{sgn}(\beta_2)(\frac{z}{L_D})}{1+(\frac{z}{L_D})^2}\frac{T^2}{T_0^2} + \frac{1}{2}\tan^{-1}(\frac{z}{L_D}) \tag{3.18}$$

The time dependence of the phase $\Phi(z, T)$ implies that the instantaneous frequency differs across the pulse from the central frequency ω_0. The difference $\delta\omega$ is just the time derivative $-\partial\Phi/\partial T$ and is given by

$$\partial\omega(T) = -\frac{\partial\phi}{\partial T} = \frac{\mathrm{sgn}(\beta_2)(\frac{2z}{L_D})}{1+(\frac{z}{L_D})^2}\frac{T}{T_0^2} \tag{3.19}$$

Equation (3.19) shows that the frequency changes linearly across the pulse, i.e., a fiber imposes linear frequency chirp on the pulse. The chirp $\delta\omega$ depends on the sign of β_2. In the normal-dispersion regime ($\beta_2 > 0$), $\delta\omega$ is negative at the leading edge ($T < 0$) and increases linearly across the pulse; the opposite occurs in the anomalous-dispersion regime ($\beta_2 > 0$).

Dispersion-induced pulse broadening occurs due to different frequency components of a pulse travel at slightly different speeds along the fiber because of GVD. Red components travel faster than blue components in the normal-dispersion regime ($\beta_2 > 0$), while the opposite phenomenon occurs in the anomalous-dispersion regime ($\beta_2 < 0$). The pulse can maintain its width only if all spectral components arrive together. Any time delay in the arrival of different spectral components leads to pulse broadening.

3.3.2 Pulse Broadening Due to GVD for Super-Gaussian Pulses

Dispersion-induced broadening is sensitive to pulse edge steepness. In general, a pulse with steeper leading and trailing edges broadens more rapidly with propagation simply because such a pulse has a wider spectrum to start with. Pulses emitted by directly modulated semiconductor lasers fall in this category and cannot generally be approximated by a Gaussian pulse. A super-Gaussian shape can be used to model the effects of steep leading and trailing edges on dispersion-induced pulse broadening. For a super-Gaussian pulse, Eq. (3.13) is generalized to take the form [25]

$$U(0,T) = \exp[-\frac{1+iC}{2}(\frac{T}{T_0})^{2m}] \tag{3.20}$$

where the parameter m controls the degree of edge sharpness. For $m = 1$ we recover the case of chirped Gaussian pulses. For larger value of m, the pulse becomes square shaped with sharper leading and trailing edges. If the rise time T_r is defined as the duration during which the intensity increases from 10 to 90% of its peak value, it is related to the parameter m as

$$T_r = (\ln 9)\frac{T_0}{2m} \approx \frac{T_0}{m} \tag{3.21}$$

Thus the parameter m can be determined from the measurements of T_r and T_0. Fig. 3.2 shows the pulse shapes at $z = 0$, L_D, and $2L_D$ in the case of an unchirped super-Gaussian pulse ($C = 0$) with $m = 3$. The differences between the two can be attributed to the steeper leading and trailing edges associated with a super-Gaussian pulse. Whereas the Gaussian pulse maintains its shape during propagation, the super-Gaussian pulse not only broadens at a faster rate but also distorts in shape. Broadening of a super-Gaussian pulse can be understood by noting that its spectrum is wider than that of a Gaussian pulse because of steeper leading and trailing edges. As the GVD-induced delay of each frequency component is directly related to its separation from the central frequency ω_0, a wider spectrum results in a faster rate of pulse broadening.

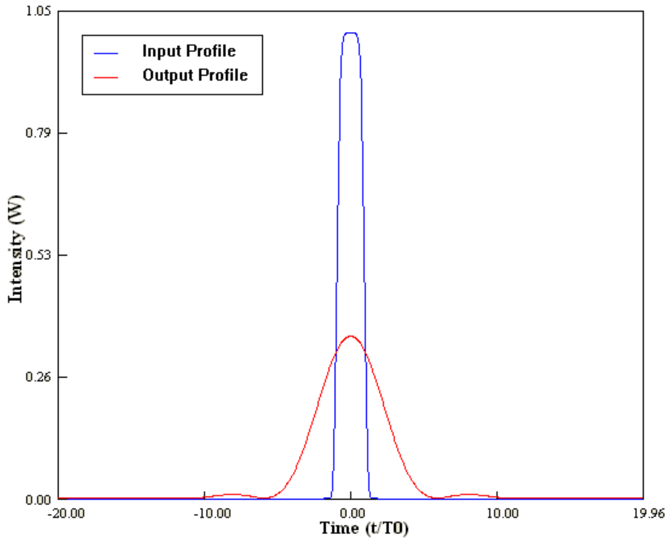

Figure 3.2: Pulse shapes at z = L_D and z = $2L_D$ of a super-Gaussian profile.

3.3.2 Changes in Pulse Shape Due to TOD Effect

The response to a Gaussian input pulse in a fiber with third-order dispersion can be expressed using the Airy function where $A_i(\gamma)$ is an Airy function. This expression is in accordance with M. Miyagi and all [26], although they followed a different approach.

$$U(z,T) = \frac{1}{2\pi} U_0 \sqrt{2\pi T_0^2} \times \int_{\infty}^{+\infty} \exp[-\frac{\omega^2 T_0^2}{2}] \exp[j(\omega T - \frac{1}{2}\beta_2 \omega^2 z - \frac{1}{6}\beta_2 \omega^3 z)] d\omega \quad (3.22)$$

Let, Q = $U_0 \sqrt{2\pi T_0^2}$, $F_1(z,\omega)$ = $\gamma = (\frac{3}{2} l)^{\frac{2}{3}}$ and $F_2(z,\omega)$ = $l = \frac{2}{9} 3^{\frac{1}{2}} \left[-\frac{t-\tau}{(-\frac{1}{6}\beta_3 z)^{\frac{1}{3}}} \right]^{\frac{3}{2}}$ (3.23)

Considering $F_1(z,\omega)$ as the Fourier Transform of a function denominated $f_1(z, \tau)$, and $F_2(z,\omega)$ as the Fourier Transform of a function denominated $f_2(z, t\text{-}\tau)$, using the convolution theorem, we obtain:

$$U(z,T)=\frac{1}{2\pi}Q\int_{-\infty}^{+\infty} f_1(z,\tau)f_2(z,t-\tau)d\tau \leftrightarrow QF_1(z,\omega)F_2(z,\omega) \quad (3.24)$$

So,

$$f_1(z,\tau)=[\frac{1}{4\pi(\frac{T_0^2}{2}+\frac{1}{2}\beta_2 z)}]^{\frac{1}{2}}\times\exp(-\frac{\tau^2}{4(\frac{T_0^2}{2}+\frac{j}{2}\beta_2 z)}) \quad (3.25)$$

This expression was obtained using the moment theorem. And

$$f_2(z,t-\tau)=\frac{1}{3}[\frac{1}{(-j(\frac{j}{6}\beta_3 z))^{\frac{1}{3}}}]\left[-\frac{t-\tau}{(j(\frac{j}{6}\beta_3 z))^{\frac{1}{3}}}\right]^{\frac{1}{2}}\frac{1}{\pi}\times besselk_{\frac{1}{3}}\left[\frac{2}{9}3^{\frac{1}{2}}\left[-\frac{t-\tau}{(-\frac{1}{6}\beta_3 z)^{\frac{1}{3}}}\right]^{\frac{3}{2}}\right]$$

(3.26)

This last expression was obtained by Matlab, solving ifourier (exp(-jaω^3)) where

$$a=\frac{j}{6}\beta_3 z \quad (3.27)$$

$$besselk_{\frac{\pm 1}{3}}(l)=\pi(\frac{3}{\gamma})Ui(\gamma) \quad (3.28)$$

$$l=\frac{2}{9}3^{\frac{1}{2}}\left[-\frac{t-\tau}{(-\frac{1}{6}\beta_3 z)^{\frac{1}{3}}}\right]^{\frac{3}{2}} \quad (3.29)$$

$$\gamma=(\frac{3}{2}l)^{\frac{2}{3}} \quad (3.30)$$

So, finally U(z,T) becomes

$$U(z,T)=\frac{1}{2\pi}Q\int_{-\infty}^{+\infty}\left[\frac{1}{4\pi(\frac{T_0^2}{2}+j\beta_2 z)}\right]\times\frac{1}{3}\frac{1}{(-\frac{1}{6}\beta_3 z)^{\frac{1}{3}}}d\tau\left[-\frac{t-\tau}{(j(\frac{j}{6}\beta_3 z))^{\frac{1}{3}}}\right]^{\frac{1}{2}}\times\left[\frac{3}{(\frac{3}{2}l)^{\frac{2}{3}}}\right]^{\frac{1}{2}}Ui(\frac{3}{2}l)^{\frac{2}{3}}d\tau$$

(3.31)

This integral has no analytical solution; its solution is numerical, substituting the variables z and t and the constants U_0, T_0, β_2 and β_3 .

Pulse evolution along the fiber depends on the relative magnitudes of β_2 and β_3, which in turn depend on the deviation of the optical wavelength λ_0 from λ_D. At $\lambda_0 = \lambda_D$, $\beta_2 = 0$, and typically $\beta_3 \approx 0.1$ ps^3/km. The TOD effects play a significant role only if $L'_D \leq L_D$ or

$T_0|\beta_2/\ \beta_3| \leq 1$. When the bit rate exceeds 10 Gb/s, both GVD and TOD have to be considered.

Fig. 3.3 shows the pulse shapes at $z = 6L'_D$ for an initially unchirped Gaussian pulse for $\beta_2 = 0$ (red curve). Whereas a Gaussian pulse remains Gaussian when only the β_2 term contributes to GVD (Fig. 3.1), the TOD distorts the pulse such that it becomes asymmetric with an oscillatory structure near one of its edges. In the case of positive β_3 shown in fig. 3.1, oscillations appear near the trailing edge of the pulse.

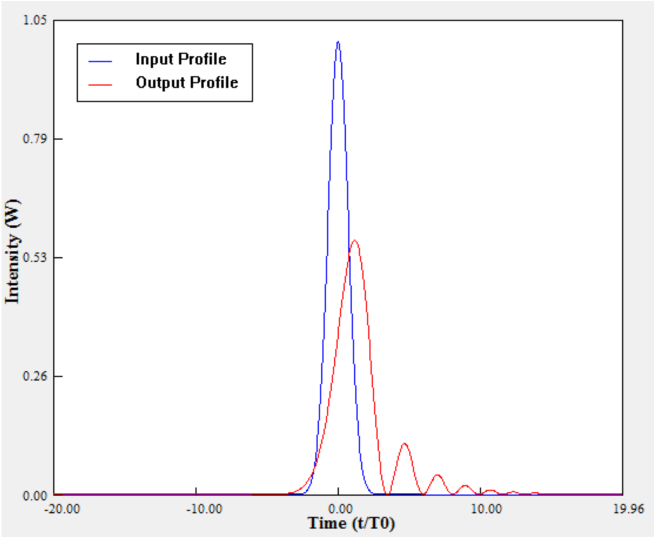

Figure 3.3: Pulse shapes at $z = 6L'_D$ of an initially Gaussian pulse at $z = 0$ (blue curve) in the presence of higher-order dispersion. Red curve shows the effect of finite β_3 when $\beta_2 = 0$.

However, these oscillations damp significantly even for relatively small values of β_2. Fig. 3.4 shows the effect of TOD for super-Gaussian pulses.

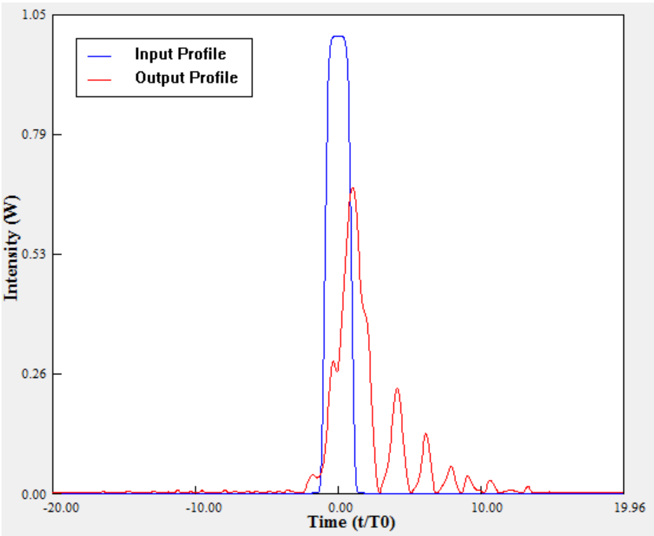

Figure 3.4: Pulse shapes at $z = 4L'_D$ of an initially Super-Gaussian pulse at $z = 0$ (blue curve) in the presence of higher-order dispersion. Red curve shows the effect of finite β_3 when $\beta_2 = 0$.

Equation (3.31) can be used to study pulse evolution for other pulse shapes (without chirp). Fig. 3.5 shows evolution of an unchirped Gaussian pulse at $\beta_3 = 0.1$.

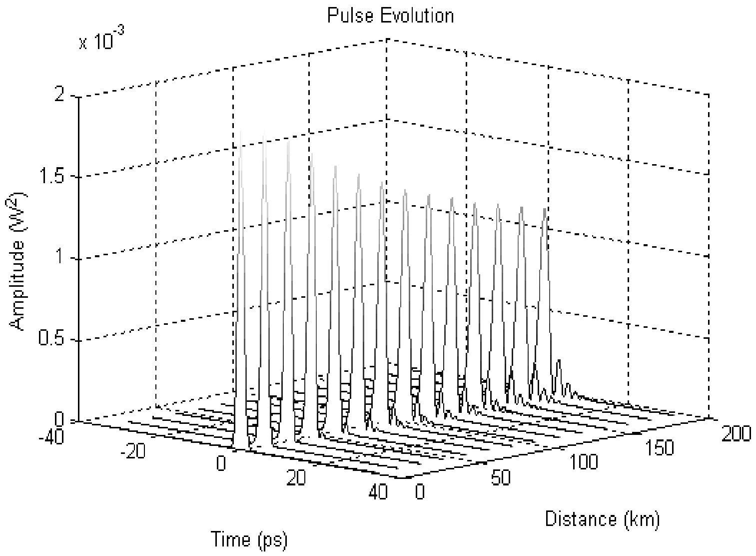

Figure 3.5: Evolution of a Gaussian pulse along the fiber length for the case of $\beta_2 > 0$ and $\beta_3 = 0.1$.

3.4 Dispersion Management Techniques

In a fiber-optic communication system, information is transmitted over a fiber by using a coded sequence of optical pulses whose width is set by the bit rate B of the system. Dispersion-induced broadening of pulses is undesirable as it interferes with the detection process and leads to errors if the pulse spreads outside its allocated bit slot ($T_B = 1/B$). Clearly, GVD limits the bit rate B for a fixed transmission distance L [6]. The dispersion problem becomes quite serious when optical amplifiers are used to compensate for fiber losses because L can exceed thousands of kilometers for long-haul systems.

When the bit rate of a single channel exceeds 100 Gb/s, the pulse spectrum becomes broad enough that it is difficult to compensate GVD over the entire bandwidth of the pulse (because of the frequency dependence of β_2). The simplest solution to this problem is provided by fibers, or other devices, designed such that both β_2 and β_3 are compensated simultaneously. For a fiber link containing two different fibers of lengths L_1 and L_2, the conditions for broadband dispersion compensation are given by

$$\beta_{21}L_1 + \beta_{22}L_{22} = 0 \, and \, \beta_{31}L_1 + \beta_{32}L_2 = 0 \quad (3.32)$$

where β_{2j} and β_{3j} are the GVD and TOD parameters for fiber of length L_j (j = 1,2).

There are several types of dispersion management techniques. Among them two of the techniques are evaluated in our thesis.

3.4.1 Dispersion Compensating Fiber (DCF)

A common method for managing dispersion is to combine two or more types of single-mode fiber to produce the desired dispersion over the entire link span. The total dispersion can be set at virtually any value as the contributions from different components may have opposite signs (i.e. either positive or negative) and hence they can partially, or completely, cancel each other. Dispersion-compensating fibers can be either placed at one location or distributed along the length of the fiber link. It consists of combining fibers with different characteristics such that the average GVD of the entire fiber link is quite low while the GVD of each fiber section is chosen to be large enough to make the four-wave-mixing effects negligible. In practice, a periodic dispersion map is used with a period equal to the amplifier spacing (typically 50–100 km). Amplifiers compensate for accumulated fiber losses in each section. Between each pair of amplifiers, just two kinds of fibers, with opposite signs of β_2, are combined to reduce the average dispersion to a small value. When the average GVD is set to zero, dispersion is totally compensated.

The implementation of fiber dispersion compensation can be done at the transmitter, at the receiver or within the fiber link. A typical transmission fiber consisted of the standard single mode fiber (SSMF) with anomalous dispersion with $D \approx 16$ ps/(km-nm) and the DCF with values of D = -100 ps/(km-nm) placed at the optical amplifier site with an amplifier at the end of each span as shown in fig. 3.6. The use of DCF for dispersion compensation was first proposed in 1980, but due to the high loss of DCFs, this technique was not applied in practice until 1990s when the Erbium-doped fiber amplifier (EDFA) was presented.

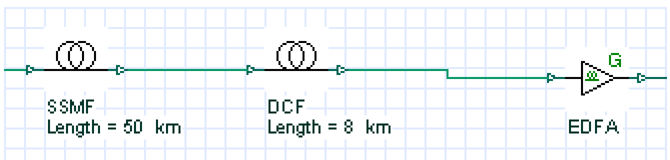

Figure 3.6: A transmission span for DM system.

Single-mode DCFs suffer from several problems. First, 1 km of DCF compensates dispersion for only 8–10 km of standard fiber. Second, DCF losses are relatively high in the 1.55-μm wavelength region ($\alpha \approx 0.5$ dB/km). Third, because of a relatively small mode diameter, the optical intensity is larger at a given input power, resulting in enhanced nonlinear effects.

Most of the problems associated with a single-mode DCF can be solved to some extent by using a two-mode fiber designed with values of V such that the higher-order mode is near cutoff ($V \approx 2.5$). Such fibers have almost the same loss as the single-mode fiber but can be designed such that the dispersion parameter D for the higher order mode has large negative values. Indeed, values of D as large as -770 ps/(km-nm) have been measured for elliptical-core fibers. A 1-km length of such a DCF can compensate the GVD of a 40-km-long fiber, adding relatively little to the total link loss. An added advantage of the two-mode DCF is that it allows for broadband dispersion compensation. However, its use requires a mode-conversion device capable of transferring radiation from the fundamental to the higher-order mode supported by the DCF. Several such all-fiber devices have been developed. As an alternative, a chirped fiber grating can be used for dispersion compensation.

3.4.2 Fiber Braggs Grating (FBG)

Dispersion compensating fiber (DCF) is currently used as the standard solution for dispersion compensation in long-haul transmission links, since it yields colorless, slope matched dispersion cancellation with negligible cascading impairments. However, DCF is also limited in optical input power to avoid nonlinear impairments, has a relatively high insertion loss and is bulky. Chirped FBGs could possibly replace DCF as the standard solution for in-line dispersion compensation. Chirped FBGs have a negligible nonlinearity, low insertion loss and small size. Wavelength Division Multiplexing (WDM) systems where multiple light signals at different frequencies are simultaneously launched in an optical fiber, the highly-selective filtering capabilities of Bragg gratings combined with its all-fiber configuration and flexibility make this technology an ideal candidate. For telecommunication applications, FBG-components have already been used for purposes such as pump laser stabilizers to improve the performances of pump lasers in optical amplifiers, gain flattening filters to equalize the gain of optical amplifiers, highly selective filters for channel selection in dense WDM systems and chromatic dispersion compensators for temporal pulse shaping in long-haul and/or high bit rate systems.

A fiber Bragg grating consists of a periodic modulation of the index of refraction along core of an optical fiber thus creating a wavelength-selective mirror as presented in fig. 3.7.

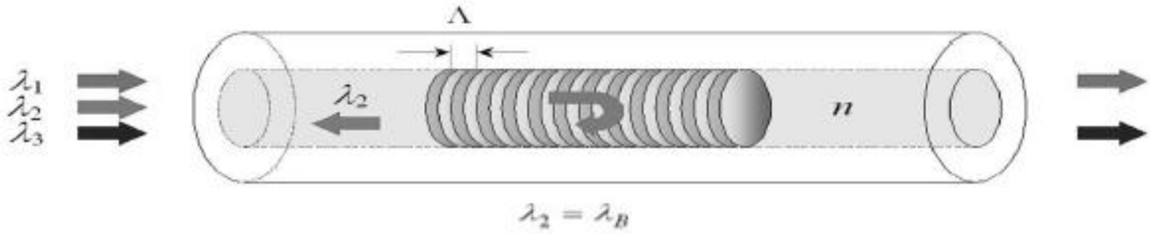

Figure 3.7: Principle of operation of FBG.

FBGs are created by the exposition of a photosensitive fiber to an intensity pattern of UV light. In its basic form, the resulting grating reflects selectively the light guided by the optical fiber at the Bragg wavelength given by:

$$\lambda B = 2n\Lambda \tag{3.33}$$

where n and Λ are the effective index of refraction of the fiber and the pitch of the grating in the fiber. A uniform grating can be represented by a sinusoidal modulation of the refractive index of the fiber core given by:

$$n(z) = n_{core} + \delta(n)[1 + \cos(2\pi z + \varphi(z)] \tag{3.34}$$

where n_{core} is the unexposed core refractive index and δn is the amplitude of the photo-induced index change. Using coupled mode theory, one can deduced the maximum reflectivity of a uniform grating at the Bragg wavelength:

$$R_{MAX}^2 = \tanh^2[\tfrac{\pi\delta L\eta}{\lambda}] \tag{3.35}$$

where L is the grating length and η is the fraction of the fiber mode power contained by the fiber core. One can see that depending on the refractive index change profile and intensity in the fiber combined with the pitch of the grating profile, numerous types of functions can be devised.

3.5 Numerical Methods for Solving NLS equation

The NLS equation is a nonlinear partial differential equation that does not generally lend itself to analytic solutions except for some specific cases in which the inverse scattering method can be employed. A large number of numerical methods can be used for this purpose. These can be classified into two broad categories known as: (i) the finite-difference methods; and (ii) the pseudospectral methods. Generally speaking, pseudospectral methods are faster by up to an order of magnitude to achieve the same accuracy. The one method that has been used extensively to solve the pulse-propagation problem in nonlinear dispersive media is the split-step Fourier method. The relative speed of this method compared with most finite-difference schemes can be attributed in part to the use of the finite-Fourier-transform (FFT) algorithm. This section describes various numerical techniques used to study the pulse-propagation problem in optical fibers with emphasis on the split-step Fourier method and its modifications.

3.5.1 Split-Step Fourier Method

To understand the philosophy behind the split-step Fourier method, it is useful to write equation formally in the form

$$\frac{\partial A}{\partial z} = (\hat{D} + \hat{N})A \tag{3.36}$$

where $\hat{D}$ is a differential operator that accounts for dispersion and absorption in a linear medium and $\hat{N}$ is a nonlinear operator that governs the effect of fiber nonlinearities on pulse propagation. These operators are given by

$$\hat{D} = -\frac{i\beta_2}{2}\frac{\partial^2}{\partial T^2} + \frac{\beta_3}{6}\frac{\partial^3}{\partial T^3} - \frac{\alpha}{2} \tag{3.37}$$

$$\hat{N} = i\gamma(|A|^2 + \frac{i}{\omega_0 A}\frac{\partial}{\partial T}(|A|^2)A - \tau_R\frac{\partial |A|^2}{\partial T}) \tag{3.38}$$

In general, dispersion and nonlinearity act together along the length of the fiber. The split-step Fourier method obtains an approximate solution by assuming that in propagating the optical field over a small distance h, the dispersive and nonlinear effects can be pretended to act independently. More specifically, propagation from z to $z + h$ is carried out in two steps. In the first step, the nonlinearity acts alone, and $\hat{D}$ =0 in Eq. (3.36). In the second step, dispersion acts alone, and $\hat{N}$ = 0 . Mathematically,

$$A(z+h,T) \approx \exp(h\hat{D})\exp(h\hat{N})A(z,T) \tag{3.39}$$

The exponential operator $\exp(h\hat{D})$ can be evaluated in the Fourier domain using the prescription

$$\exp(h\hat{D})B(z,T) = F^{-1}\exp[h\hat{D}(i\omega)F_T B(z,T)] \tag{3.40}$$

where FT denotes the Fourier-transform operation, $\hat{D}(i\omega)$ is obtained from Eq. (3.40) by replacing the differential operator $\partial = \partial$ T by iω, and ω is the frequency in the Fourier domain. As $\hat{D}(i\omega)$ is just a number in the Fourier space, the evaluation of Eq. (3.40) is straightforward. The use of the FFT algorithm makes numerical evaluation of Eq. (3.40) relatively fast.

To estimate the accuracy of the split-step Fourier method, we note that a formally exact solution of Eq. (3.36) is given by

$$A(z+h,T) = \exp[h(\hat{D}+\hat{N})]A(z,T) \tag{3.41}$$

If $\hat{N}$ is assumed to be *z* independent. At this point, it is useful to recall the Baker–Hausdorff formula for two non-commuting operators $\hat{a}$ and $\hat{b}$.

$$\exp(\hat{a})\exp(\hat{b}) = \exp(\hat{a}+\hat{b}+\tfrac{1}{2}[\hat{a},\hat{b}]+\tfrac{1}{12}[\hat{a}-\hat{b},[\hat{a},\hat{b}]]) \tag{3.42}$$

where $[\hat{a},\hat{b}] = \hat{a}\hat{b} - \hat{b}\hat{a}$ A comparison of Eqs. (3.40) and (3.42) shows that the split-step Fourier method ignores the non-commutating nature of the operators $\hat{D}$ and $\hat{N}$. By using Eq. (3.42) with $\hat{a} = h\hat{D}$ and $\hat{b} = h\hat{N}$ the dominant error term is found to result from the single commutator $\tfrac{1}{2}h^2[\hat{D},\hat{N}]$ Thus, the split step Fourier method is accurate to second order in the step size *h*.

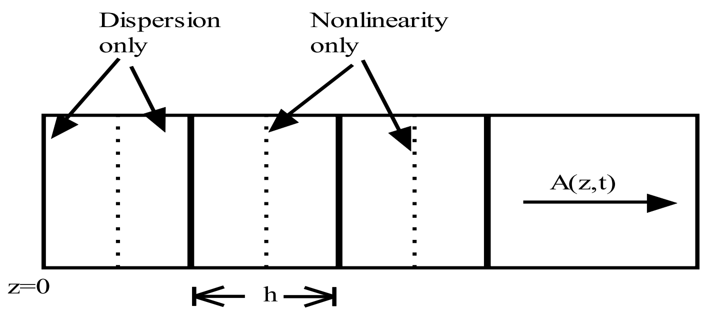

Figure 3.8: Schematic illustration of the symmetrized split-step Fourier method used for numerical simulations. Fiber length is divided into a large number of segments of width *h*. Within a segment, the effect of nonlinearity is included at the mid-plane shown by a dashed line.

The fiber length is divided into a large number of segments that need not be spaced equally. The optical pulse is propagated from segment to segment using the prescription of Eq. (3.42). More specifically, the optical field $A(z, T)$ is first propagated for a distance $h = 2$ with dispersion only using the FFT algorithm. At the mid-plane $z + h = 2$, the field is multiplied by a nonlinear term that represents the effect of nonlinearity over the whole segment length h. Finally, the field is propagated the remaining distance $h = 2$ with dispersion only to obtain $A(z + h, T)$. In effect, the nonlinearity is assumed to be lumped at the mid-plane of each segment (dashed lines in Fig. 3.8). The time window should be wide enough to ensure that the pulse energy remains confined within the window. Typically, window size is 10–20 times the pulse width. In general, the split-step Fourier method is a powerful tool provided care is taken to ensure that it is used properly.

3.6 Evaluating System Performances

3.6.1 Eye Diagram

The eye diagram is an overlay of many transmitted waveforms. By using a clock signal as the trigger input to the digital sampling oscilloscope, the transmitted waveform can be sampled over virtually the entire data pattern generated by the transmitter. Thus, all the various bit sequences that might be encountered can be sampled to build-up a eye diagram.

Eye pattern is called Eye diagram, since visual representation of pattern is in the shape of an eye. Eye-pattern technique is a method, which is used to asses maximum transmission rate of a system .Major application of eye pattern is in the optical fiber data links. Eye pattern is measured in time domain and an oscilloscope is used to view the effects of distorted signal. Eye pattern is combination of repeated signals samples generated at output.

In fig. 3.9 and fig. 3.10, difference between a degraded and ideal eye pattern is shown.

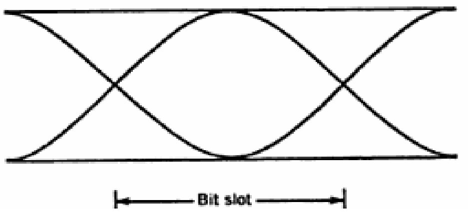

Figure 3.9: Ideal eye pattern.

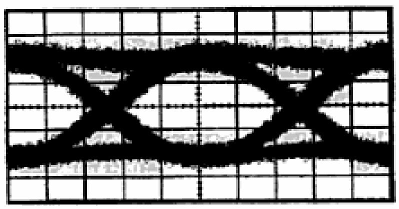

Figure 3.10: Degraded eye pattern.

3.6.2 Bit Error Ratio (BER) Measurements

BER is the average probability of incorrect bit identification of a bit by decision circuit of the receiver for a specified time interval or quantity of bits. A commonly used criterion for digital optical receivers requires BER of less than 1x 10^{-9}.Bit error rate is defined as number of errors occurring over a certain period of time by total number of pulses transmitted during this interval. The error rate depends on signal to noise ratio determined by Q factor. The relation between BER and Q factor is given by

$$BER = \left(\frac{1}{\sqrt{2\pi}} \right) \left(\frac{e^{-\frac{Q^2}{2}}}{Q} \right) \tag{3.43}$$

If Q factor of the system or design increases then BER decreases, means signal received with small noise factor at receiver.

3.7 Conclusion

Mathematical and simulation analysis of GVD and TOD were presented. The evolution of the pulse was discussed in the presence of GVD and TOD individually in the absence of fiber loss and fiber nonlinearity. The effect of TOD is seen by applying an analytic technique over basic pulse equation that is NLSE. This is done by the method used by M. Miyagi [26]. The results presented in this chapter were obtained through a numerical model of pulse propagation and were found consistent with the results already given in the literature. These results have also shown the well known fact that it is necessary to consider both GVD and TOD during pulse propagation through optical fiber when bit rate exceeds over 10 Gb/s.

Chapter 4

Simulation Tools and Models

4.1 Introduction to OptiSystem Tool

OptiSystem is an innovative optical communication system simulation package that designs, tests, and optimizes virtually any type of optical link in the physical layer of a broad spectrum of optical networks, from analog video broadcasting systems to intercontinental backbones. OptiSystem is a stand-alone product that does not rely on other simulation frameworks. It is a system level simulator based on the realistic modeling of fiber-optic communication systems. It possesses a powerful new simulation environment and a truly hierarchical definition of components and systems. Its capabilities can be extended easily with the addition of user components, and can be seamlessly interfaced to a wide range of tools.

A comprehensive Graphical User Interface (GUI) controls the optical component layout and netlist, component models, and presentation graphics. The extensive library of active and passive components includes realistic, wavelength-dependent parameters. Parameter sweeps allow investigating the effect of particular device specifications on system performance. OptiSystem is also available in two additional configurations:

•Amplifier Edition

•Multimode Edition

4.1.1 Benefits

•Rapid, low-cost prototyping

•Global insight into system performance

•Straightforward access to extensive sets of system characterization data

•Automatic parameter scanning and optimization

•Assessment of parameter sensitivities aiding design tolerance specifications

•Dramatic reduction of investment risk and time-to-market

•Visual representation of design options and scenarios to present to prospective customers

4.1.2 Applications

OptiSystem allows for the design automation of virtually any type of optical link in the physical layer, and the analysis of a broad spectrum of optical networks, from long-haul systems to MANs and LANs.

OptiSystem's wide range of applications include:

•Optical communication system design from component to system level at physical layer

•CATV or TDM/WDM network design

•Passive optical networks (PON) based FTTx

•Free space optic (FSO) systems

•Radio over fiber (ROF) systems

•SONET/SDH ring design

•Transmitter, channel, amplifier, and receiver design

•Dispersion map design

•Estimation of BER and system penalties with different receiver models

•Amplified system BER and link budget calculations

4.2 System Set Up

The choice of modulation format has an important performance/economic tradeoff. From a performance standpoint, the best modulation format is dictated by many system parameters, such as system length, the fiber type, the dispersion management, and the optical bandwidth. One of the key challenges of the system design is to transmit a pulse shape that will survive the long transmission distance in the presence of dispersion, fiber nonlinearity and the added optical noise from the amplifiers. Transmission based on this simple on/off pulse scheme is referred to a unipolar pulse system. When the shape of the light pulse used is a rectangular pulse that occupies the entire bit period, the format is referred to as a Non-Return-to-Zero (NRZ) format. Strings of binary data with optical pulses that do not occupy the entire bit period are described generically as Return-to-Zero (RZ). Much attention has been focused recently on the use of RZ signaling because of its demonstrated improved immunity to fiber nonlinearities related to NRZ. If rectangular pulses were generated with a pulse width half the bit time, their spectral occupancy would be twice that of NRZ, as the first nulls in the frequency domain would occur at +/-2*B*, relative to the optical carrier, and their potential spectral efficiency would be one half that of NRZ signals. But as the RZ format occupies twice the spectral width of NRZ format, it will be more severely effected by the chromatic dispersion.

Single- channel 100 Gb/s transmission over SSMF and DCF with RZ modulation format is illustrated schematically in fig. 4.1.

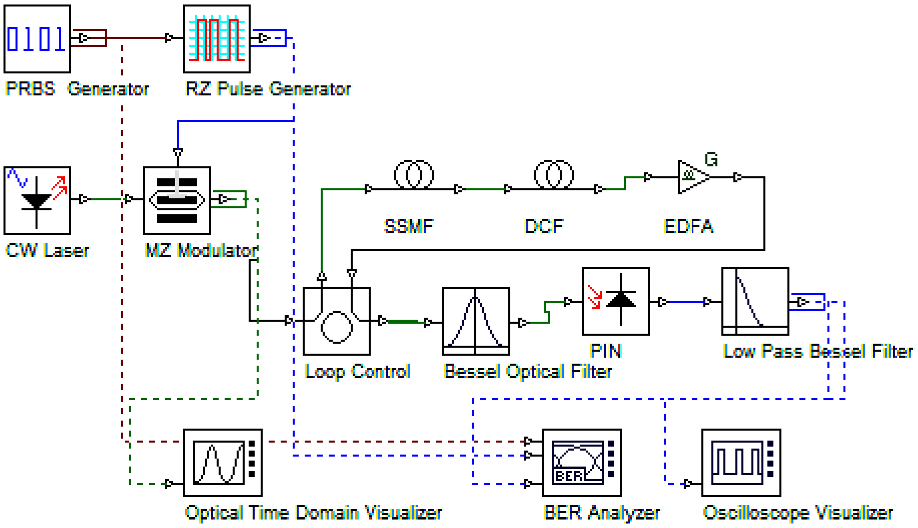

Figure 4.1: Schematic Diagram of 100 Gb/s RZ pulse Dispersion Compensated System.

4.2.1 Transmitter Section

The transmitter section shown in fig. 4.2 is composed of data source, electrical driver, laser source, amplitude modulator.

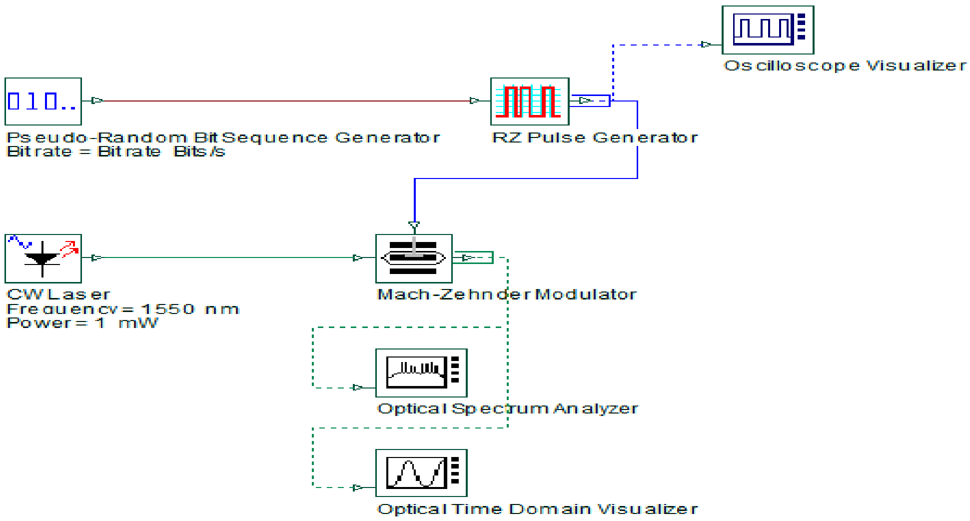

Figure 4.2: Set up of 100 Gb/s RZ pulse used for transmission.

Data Source:

Data Source (user-defined bit sequence generator) stimulates a bit sequences that is user defined. In our simulation, bit sequence is 0000010000. The sequence length is defined by:

$$N = T_w B_r \tag{4.1}$$

T_w is the global parameter Time window and B_r is the parameter Bit rate. If the user-defined sequence is shorter than the *N*, the sequence will be repeated until the length is equal to *N*. Data source or logical signal is customized by bit rate, bit sequence, sample rate, sequence length, number of samples, etc.

Electrical Pulse Generator:

Logical signal is passed to the electrical pulse generator which converts the logical signal, a binary sequence of zeros and ones into an electrical signal. In this transmitter set up, RZ pulse generator has been used. Properties of RZ pulse generator are shown in table-1.

Table 1: Properties of RZ Pulse Generator

Main | Simulation

Disp	Name	Value	Units	Mode
☐	Rectangle shape	Gaussian		Normal
☐	Amplitude	1	a.u.	Normal
☐	Bias	0	a.u.	Normal
☐	Duty cycle	0.5	bit	Normal
☐	Position	0	bit	Normal
☐	Rise time	0.05	bit	Normal
☐	Fall time	0.05	bit	Normal

According to the parameter Rectangle shape, this model can produce pulses with different edge shapes such as exponential, Gaussian, linear and sine. In our simulation, we have used Gaussian shape which is defined as

$$E(t) = \begin{cases} 1 - \exp(-\frac{t}{c_r})^2, 0 \le t < t_1 \\ 1, t_1 \le t < t_2 \\ \exp(-\frac{t}{c_f})^2, t_2 \le t < t_c \\ 0, t_c \le t < T \end{cases} \tag{4.2}$$

where c_r is the rise time coefficient and c_f is the fall time coefficient. t_1 and t_2, together with c_r and c_f, are numerically determinate to generate pulses with the exact values of the parameters Rise time and Fall time. t_c is the duty cycle duration, and T is the bit period.

Laser Source:

Laser source provides transmission at 1550 nm laser emission frequency. In the simulation, CW laser has been used. CW laser generates a continuous wave (CW) optical signal. Properties of CW laser are given in the following table 2.

Table 2: Properties of CW laser

Main | Polarization | Simulation | Noise | Random numbers

Disp	Name	Value	Units	Mode
☑	Frequency	1550	nm	Normal
☑	Power	1	mW	Sweep
☐	Linewidth	0.1	MHz	Normal
☐	Initial phase	0	deg	Normal

Amplitude Modulator:

The output from electrical driver and laser source is passed to an amplitude modulator. The Mach-Zehnder (MZ) modulator is an intensity modulator based on an interferometric principle. It consists of two 3 dB couplers which are connected by two waveguides of equal length. By means of an electro-optic effect, an externally applied voltage can be used to vary the refractive indices in the waveguide branches. The electrical input signal is normalized between 0 and 1. MZ modulator has the following properties:

Table 3: Properties of MZ modulator

Main | Simulation

Disp	Name	Value	Units	Mode
☐	Extinction ratio	30	dB	Normal
☐	Negative signal chirp	☐		Normal
☐	Symmetry factor	-1		Normal

4.2.2 Optical Link Section:

The optical signal MZ external modulator is passed through the optical link section. The optical link is composed of different spans of 50 Km SSMF, 8 Km DCF for dispersion compensation and in-line EDFA for loss compensation and loop control as shown in fig. 4.3.

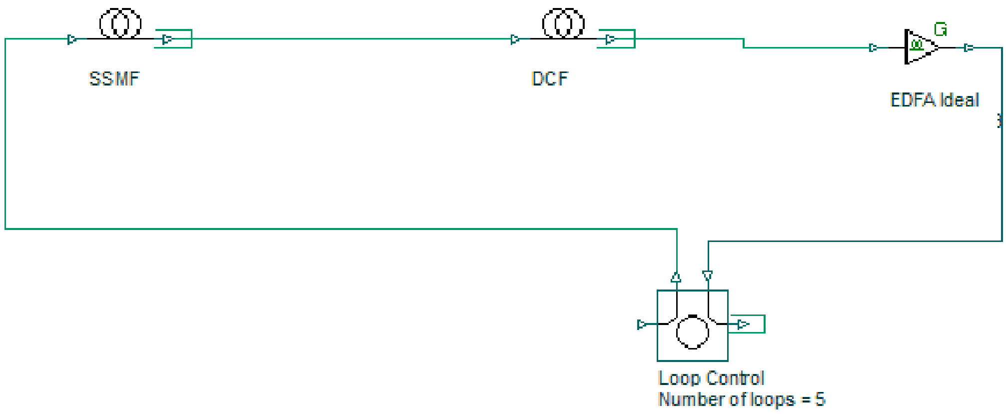

Figure 4.3: Components of Optical Link Section.

Optical Fibers:

The optical fiber component simulates the propagation of an optical field in a single-mode fiber with the dispersive and nonlinear effects taken into account by a direct numerical integration of the modified nonlinear Schrödinger (NLS) equation (when the scalar case is considered) and a system of two, coupled NLS equations when the polarization state of the signal is arbitrary. The optical sampled signals reside in a single frequency band, hence the name total field. The parameterized signals and noise bins are only attenuated.

The properties of different types of fibers are shown below

(i) SSMF:

Table 4: Properties of SSMF Fiber

Main | Disp... | PMD | Nonl... | Num... | Gr... | Simu... | Noise | Rand...

Disp	Name	Value	Units	Mode
☐	User defined reference w	☑		Normal
☐	Reference wavelength	1550	nm	Normal
☑	Length	100	km	Normal
☐	Attenuation effect	☑		Normal
☐	Attenuation data type	Constant		Normal
☐	Attenuation	0.2	dB/km	Normal
☐	Attenuation vs. wavelengt	Attenuation.dat ...		Normal

Disp	Name	Value	Units	Mode
☐	Group velocity dispersion	☑		Normal
☐	Third-order dispersion	☑		Normal
☐	Dispersion data type	Constant		Normal
☐	Frequency domain param	☐		Normal
☐	Dispersion	16	ps/nm/km	Normal
☐	Dispersion slope	0.08	ps/nm^2/k	Normal
☐	Beta 2	-20	ps^2/km	Normal
☐	Beta 3	0	ps^3/km	Normal

Disp	Name	Value	Units	Mode
☐	Self-phase modulation	☑		Normal
☐	Effective area data type	Constant		Normal
☐	Effective area	80	um^2	Normal
☐	Effective area vs. wavelen	EffectiveAra.dat ...		Normal
☐	n2 data type	Constant		Normal
☐	n2	2.6e-020	m^2/W	Normal
☐	n2 vs. wavelength	n2.dat ...		Normal
☐	Self-steepening	☐		Normal
☐	Full Raman Response	☐		Normal
☐	Intrapulse Raman Scatt.	☐		Normal
☐	Raman self-shift time1	14.2	fs	Normal
☐	Raman self-shift time2	3	fs	Normal
☐	Fract. Raman contribution	0.18		Normal
☐	Orthogonal Raman factor	0.75		Normal

(ii) DCF:

Table 5: Properties of DCF Fiber

Main | Disp... | PMD | Nonl... | Num... | Gr... | Simu... | Noise | Rand...

Disp	Name	Value	Units	Mode
☐	User defined reference w	☑		Normal
☐	Reference wavelength	1550	nm	Normal
☑	Length	20	km	Normal
☐	Attenuation effect	☑		Normal
☐	Attenuation data type	Constant		Normal
☐	Attenuation	0.5	dB/km	Normal
☐	Attenuation vs. wavelengt	Attenuation.dat ...		Normal

Disp	Name	Value	Units	Mode
☐	Group velocity dispersion	☑		Normal
☐	Third-order dispersion	☑		Normal
☐	Dispersion data type	Constant		Normal
☐	Frequency domain param	☐		Normal
☐	Dispersion	-80	ps/nm/km	Normal
☐	Dispersion slope	0.08	ps/nm^2/k	Normal
☐	Beta 2	-20	ps^2/km	Normal
☐	Beta 3	0	ps^3/km	Normal

Disp	Name	Value	Units	Mode
☐	Self-phase modulation	☑		Normal
☐	Effective area data type	Constant		Normal
☐	Effective area	23	um^2	Normal
☐	Effective area vs. wavelen	EffectiveAra.dat		Normal
☐	n2 data type	Constant		Normal
☐	n2	3e-020	m^2/W	Normal
☐	n2 vs. wavelength	n2.dat		Normal
☐	Self-steepening	☐		Normal
☐	Full Raman Response	☐		Normal
☐	Intrapulse Raman Scatt.	☐		Normal
☐	Raman self-shift time1	14.2	fs	Normal
☐	Raman self-shift time2	3	fs	Normal
☐	Fract. Raman contribution	0.18		Normal
☐	Orthogonal Raman factor	0.75		Normal

Optical Amplifier:

An optical amplifier is a device that amplifies an optical signal directly, without the need to first convert it to an electrical signal. An optical amplifier may be thought of as a laser without an optical cavity, or one in which feedback from the cavity is suppressed. There are several different physical mechanisms that can be used to amplify a light signal, which correspond to the major types of optical amplifiers. In doped fiber amplifiers and bulk lasers, stimulated emission in the amplifier's gain medium causes amplification of incoming light. In semiconductor optical amplifiers (SOAs), electron-hole recombination occurs. In Raman amplifiers, Raman scattering of incoming light with phonons in the lattice of the gain medium produces photons coherent with the incoming photons. Parametric amplifiers use parametric amplification.

Erbium-doped fiber amplifiers are the by far most important fiber amplifiers in the context of long-range optical fiber communications; they can efficiently amplify light in the 1.5-µm wavelength region, where telecom fibers have their loss minimum.

In the Optisystem, black box model designs Er-doped fiber amplifiers by considering numerical solutions of the rate and the propagation equations under stationary conditions. The model includes amplified spontaneous emission (ASE) as observed in the amplifier Erbium Doped Fiber. However, this module allows one to select forward and/or backward pump, as well as the pump power values.

Three different control modes are available that allow to perform the amplifier analysis under distinct points of view. Each mode control – gain, power control, and saturation – defines a different amplifier operating condition. In our simulation, we have used the gain control mode. Properties of EDFA amplifier used in the simulation are given below-

Table 6: Properties of EDFA Amplifier

Main | Polarization | Simulation | Noise | Random numbers

Disp	Name	Value	Units	Mode
☐	Operation mode	Gain Control		Normal
☑	Gain	30	dB	Normal
☐	Power	10	dBm	Normal
☐	Saturation power	10	dBm	Normal
☐	Saturation port	Output		Normal
☐	Include noise	☐		Normal
☐	Noise figure	6	dB	Normal

Disp	Name	Value	Units	Mode
☐	Noise center frequency	193.4	THz	Normal
☐	Noise bandwidth	13	THz	Normal
☐	Noise bins spacing	125	GHz	Normal
☐	Convert noise bins	Convert noise bins S		Script

Loop Control:

It allows building systems using loop structures. The loop topology starts at the Loop output port and terminates at the Loop input port. The signal enters the Input port and circulates in the loop N times, where N is defined by the parameter Number of Loops.

4.2.3 Receiver Section

Receiver section consists of optical filter, photo-detector and electrical filter as shown in fig. 4.4.

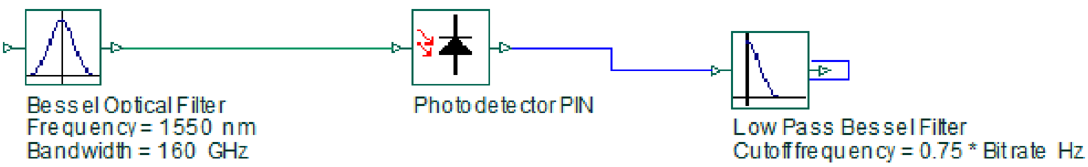

Figure 4.4: Components of receiver Section.

Optical Filter:

Optical filters are devices that selectively transmit light of different wavelengths, usually implemented as plane glass or plastic devices in the optical path which are either dyed in the mass or have interference coatings. Optical filters selectively transmit light in a particular range of wavelengths, that is, colours, while blocking the remainder. They can usually pass long wavelengths only (long pass), short wavelengths only (short pass), or a band of wavelengths, blocking both longer and shorter wavelengths (band pass). The pass-band may be narrower or wider; the transition or cutoff between maximal and minimal transmission can be sharp or gradual. 100Gb/s system is simulated using Bessel optical filter. Bessel optical filter is an optical filter with a Bessel frequency transfer function. Properties of Bessel optical filters are given as follows-

Table 7: Properties of Bessel optical filter

Main | Simulation | Noise

Disp	Name	Value	Units	Mode
☐	Frequency	1550	nm	Normal
☐	Bandwidth	160	GHz	Normal
☐	Insertion loss	0	dB	Normal
☐	Depth	100	dB	Normal
☐	Order	1		Normal

Photo-detector:

The incoming optical signal and noise bins are filtered by an ideal rectangle filter to reduce the number of samples in the electrical signal. The sensitivity of a receiver can be defined by optimizing the receiver parameters. A typical parameter of BER is10^{-9}. Properties or pin photo-detector is shown in table-8:

Table 8: Properties of pin photo-detector

Main | Downsampling | Noise | Random numbers

Disp	Name	Value	Units	Mode
☐	Responsivity	1	A/W	Normal
☐	Dark current	10	nA	Normal

Main | Downsampling | Noise | Random numbers

Disp	Name	Value	Units	Mode
☐	Noise calculation type	Numerical		Normal
☐	Add signal-ASE noise	☑		Normal
☐	Add ASE-ASE noise	☑		Normal
☐	Add thermal noise	☑		Normal
☐	Thermal noise	1e-024	W/Hz	Normal
☐	Add shot noise	☑		Normal
☐	Shot noise distribution	Gaussian		Normal

Electrical Filter:

The output of the pin photo-detector is the electrical signal. This electrical signal is filtered with low-pass Bessel electric filter in the set up. Low-pass Bessel electric filter has the following properties:

Table 9: Properties of low-pass Bessel electrical filter

Disp	Name	Value	Units	Mode
☑	Cutoff frequency	0.75 * Bit rate	Hz	Script
☐	Insertion loss	0	dB	Normal
☐	Depth	100	dB	Normal
☐	Order	4		Normal

4.2.4 Visualizing Components:

At transmitter and receiver, measurements are made with the help of optical time and spectrum analyzers, oscilloscope visualizer, eye diagram and BER analyzers.

Optical Spectrum Analyzer (OSA):

This visualizer allows the user to calculate and display optical signals in the frequency domain. It can display the signal intensity, power spectral density, phase, group delay and dispersion for polarizations X and Y.

Optical Time Domain Visualizer (OTDV):

This visualizer allows the user to calculate and display optical signals in the time domain. It can display the signal intensity, frequency.

Oscilloscope Visualizer:

This visualizer allows the user to calculate and display electrical signals in the time domain. It can display the signal amplitude and autocorrelation.

Eye Diagram Analyzer:

This visualizer allows the user to calculate and display the electrical signal eye diagram automatically. It can calculate different metrics from the eye diagram, such as Q factor, eye opening, eye closure, extinction ratio, eye height, mask violation ratio, etc. It can also display histograms and standard eye masks.

BER Analyzer:

This visualizer allows the user to calculate and display the bit error rate (BER) of an electrical signal automatically. It can estimate the BER using different algorithms such as Gaussian and Chi-Squared and derive different metrics from the eye diagram, such as Q factor, eye opening, eye closure, extinction ratio, eye height, jitter, etc.

Chapter 5

Results and Discussions

5.1 Introduction

In this chapter, at first, pulse broadening due to GVD and TOD has been observed by varying bit rates from 40 Gb/s to 160 Gb/s. Then temporal shift of pulse center position is investigated by varying transmission distance, bit rate, duty cycle, input pulse shape and different transmission models for DM systems. Finally, performance of input pulses such as Gaussian and super-Gaussian pulses is evaluated by varying bit rates from 40 Gb/s to 160 Gb/s. Fiber chromatic dispersion, SPM and receiver noises are assumed for the numerical calculation. DM transmission line is considered for each scheme. A PRBS of length 2^7-1 is used to propagate through the optical fiber. Finally, FBG as TOD compensator has been used for different high bit rate systems (100 Gb/s, 160 Gb/s and 320 Gb/s).

5.2 Effects of GVD and TOD in Ultra High-Speed Optical Fiber Communication System

Even if the transmission bandwidth is limited to a single channel, TOD causes to have pulse ripples in ultra high-speed optical transmission systems. Fig. 5.1 shows pulse evaluation through SSMF for 100Gb/s when when both GVD and TOD are present.

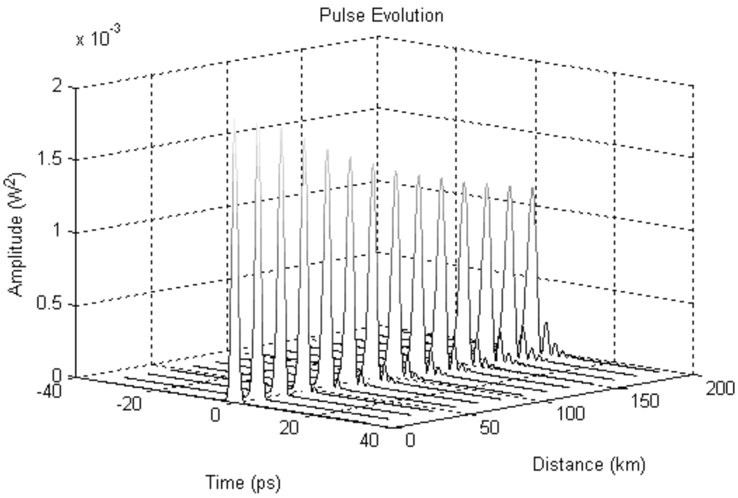

Figure 5.1: Pulse Evolution through SSMF when both GVD and TOD are present.

Gaussian pulse evolution in single fiber transmission system for a transmission period of 200 km has been numerically simulated using Matlab. The codes are included in appendix. Pulse evolution along SSMF in the absence of noise has been observed considering both GVD and TOD effects in fig. 5.1. It is evident from fig.5.1 that each pulse is spreading out as it propagates down the fiber.

Effect of TOD for pulse evolution through dispersion shifted fiber (DSF) for different bit-rates is also observed using Matlab. The numerical results are shwn in fig. 5.2.

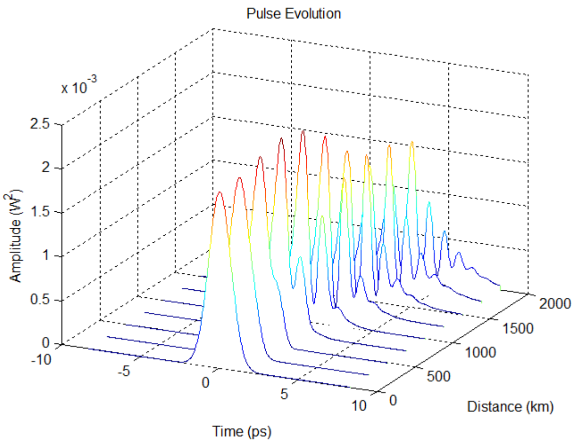

Bit Rate: 40Gbps
D = 40%
$\beta_3 = 0.1462 ps^3/km$
Fiber length (km) : 2000

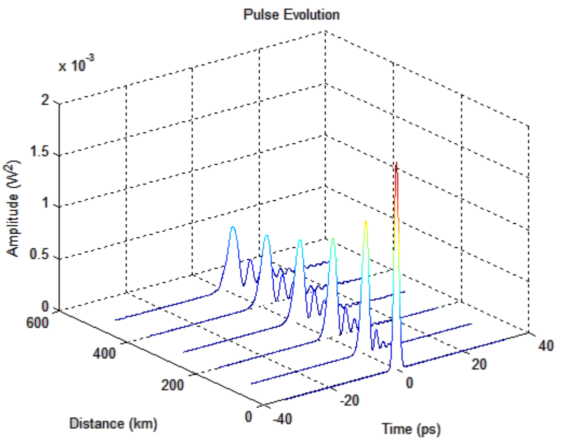

Bit Rate: 160Gbps
D = 40%
$\beta_3 = 0.1462 ps^3/km$
Fiber length (km) : 500

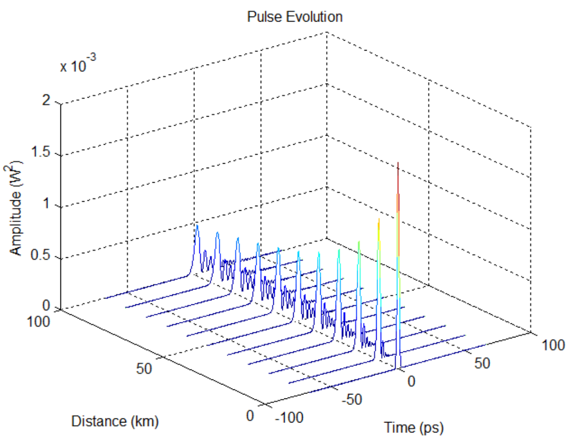

Bit Rate: 320Gbps
D = 40%
$\beta_3 = 0.1462 ps^3/km$
Fiber length (km) : 100

Figure 5.2: Pulse Evolution through DSF for different bit rates.

From, fig. 5.1 and 5.2, it is found that GVD is the main factor limiting transmission length in high-speed optical single-mode fibre systems; it reduces significantly the amplitude and broadens the time width of the pulses for systems operating at speeds higher or equal to 40 Gbit/s. TOD distorts the pulse and the pulse becomes asymmetric with an oscillatory structure near one of its edges.

5.2.1 Impact of TOD on Bit Rates

In the first simulation TOD effect is observed for the Gaussian and super-Gaussian pulses propagating through SSMF-DCF system by varying bit rates only. Incident power is 1 mW and duty cycle is 50%. Bit rate is varied from 40 Gb/s to 160 Gb/s. Propagation distance was upto 2030 km.

In the simulation, third order super-Gaussian pulse has been used to reduce timing jitter in the system. Increasing the bit rate will decrease the pulse width, thus making the bits more sensitive to dispersion effect. With the increase of bit rates, TOD effect also increases as TOD dispersion length (L_{D3}) becomes smaller than that of GVD which in turn satisfies the condition for TOD effect i.e. $L_{D3} < L_{D2}$ as shown in fig. 5.3.

For 40 Gb/s, TOD effect is negligible as evident from fig. 5.3(a) and 5.3(b). In case of 100 Gb/s, the pulse broadens to almost 10 ps from 5 ps (FWHM) for Gaussian pulse after transmission of 2030 km and exhibits a long oscillatory tail extending around 40 ps for both Gaussian and super-Gaussian pulse shapes as shown in fig. 5.3(c) and 5.3(d). For 160 Gb/s, pulse broadens to almost 6 ps from 3.125 ps (FWHM) for Gaussian pulse and oscillatory tail is found on both edges of pulse which extends around 60 ps as shown in fig. 5.3(e) and 5.3(f). It has been made clear that TOD changes DM system's group velocity, leads to emission continuum radiation, and makes pulse's shape asymmetric. Effect of TOD is dominant in case of super Gaussian pulse shape as it has steeper leading and trailing edges than those of Gaussian pulse.

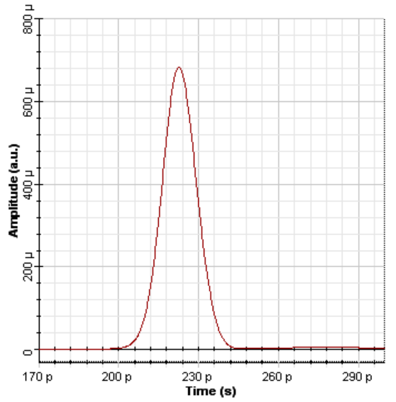

(a)

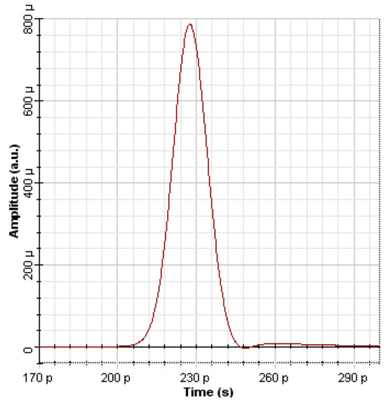

(b)

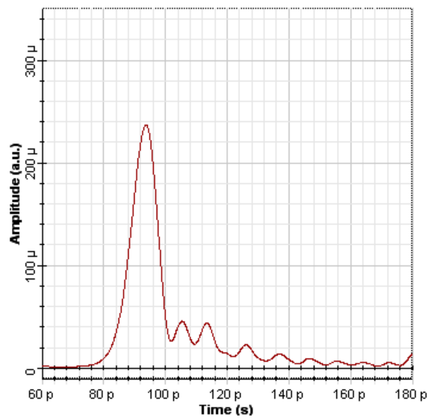

(c)

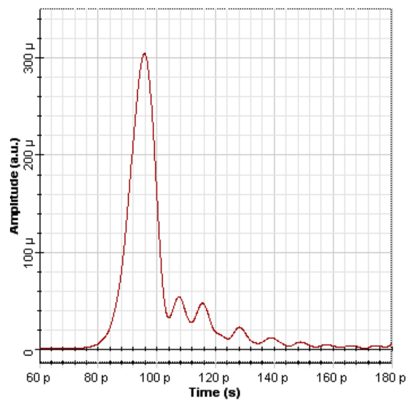

(d)

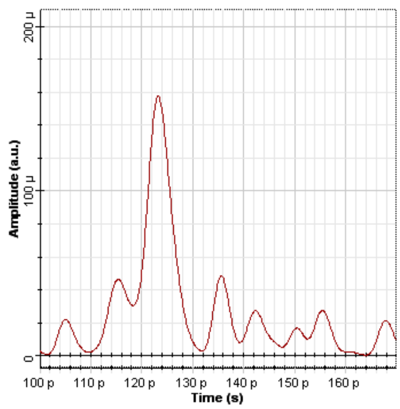

(e)

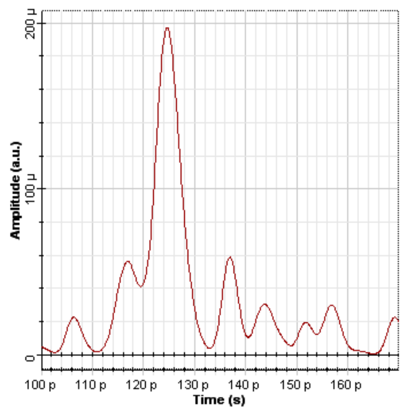

(f)

Figure 5.3: Pulse Propagation through SSMF-DCF at transmission distance of 2030 km for (a) 40 Gb/s Gaussian (b) 40 Gb/s Super Gaussian (c) 100 Gb/s Gaussian (d) 100 Gb/s Super Gaussian (e) 160 Gb/s Gaussian (f) 160 Gb/s Super Gaussian.

5.3 Effect of TOD on Pulse Center Position

5.3.1 Changes of Pulse Center Position for Different Bit Rates

In second simulation we compare the temporal shift of pulse center of RZ Gaussian pulses with duty cycle of 50% in DM system by increasing the bit rate from 40 Gb/s to 160 Gb/s to check the effects of TOD. At first, impact of pulse center position was observed for Gaussian and super-Gaussian pulse shapes considering only GVD effect for a particular bit rate. Then the same outcome was observed considering both GVD and TOD effects for the corresponding bit rate. The results are shown in fig. 5.4.

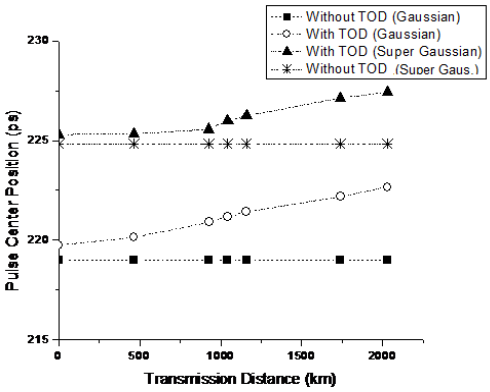

(a)

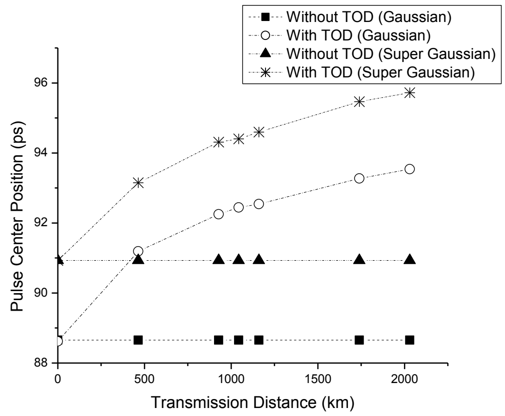

(b)

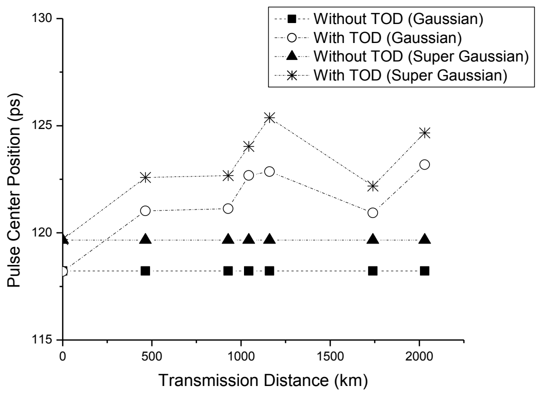

(c)

Figure 5.4: Changes of pulse center position with variations of propagation distance- (a) 40 Gb/s RZ Gaussian (b) 100 Gb/s RZ Gaussian (c) 160 Gb/s RZ Gaussian pulses.

With the change of bit rates, pulse center position remains unchanged when only GVD is considered for pulse propagation. But, when TOD is considered, pulse center position changes with the variation of transmission distance.

The effect of TOD on pulse center position is shown in fig.5.4. For 40 Gb/s, pulse center shifts to 2.926 ps for RZ Gaussian pulse and 2.123 ps for super-Gaussian pulse after transmission distance of 2030 km. It implies that TOD causes the temporal right shift of the optical pulses from its initial position for the changes of transmission distance which can also be verified by the equation used (3.31). Variations of pulse center position increases with the increase of bit rates and this effect dominates slightly more on Gaussian pulse shape rather than super-Gaussian pulse as shown in fig. 5.5. For 100 Gb/s and 160 Gb/s Gaussian pulses these variations are 4.9196 ps and 4.984 ps, respectively and 4. 931 ps and 4.977 ps, respectively for super-Gaussian pulses as shown in fig. 5.3(b) and 5.3(c). Summary of the results are shown in table-10.

Table-10: Change of pulse center position (ps)

	Gaussian		Super Gaussian	
B (Gb/s)	GVD only	GVD+TOD	GVD only	GVD+TOD
40	0	2.926	0	2.123
100	0	4.9496	0	4.931
160	0	4.984	0	4.977

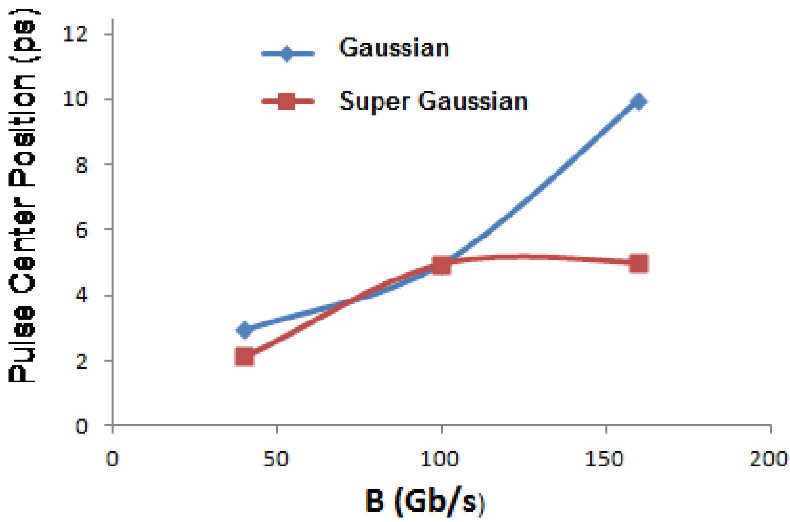

Figure 5.5: Changes of pulse center position with variations of bit rates for RZ Gaussian and super Gaussian pulses.

However, for higher bit rates Q-factor of Gaussian pulses is better than that of super-Gaussian pulses at a particular distance of 2030 km. The results are shown in table-11.

TABLE-11: BER AND Q-FACTOR FOR DIFFERENT INCIDENT PULSES WITH DIFFERENT BIT RATES

Pulse Shape	Transmission Distance = 2030 km			
	100 Gb/s		160 Gb/s	
	Q (dB)	**BER**	**Q (dB)**	**BER**
Gaussian	7.24	2.24×10^{-13}	6.732	6.99×10^{-12}
Super Gaussian	6.12	4.3×10^{-10}	5.832	1.84×10^{-9}

5.3.2 Changes of Pulse Center Position for the Variation of Duty Cycles

In the next simulation, the shift of pulse center position due to TOD has been observed for 100 Gb/s RZ Gaussian pulse by varying duty cycles (D) from 20% to 80% and transmission reach as shown in fig. 5.6. Here, SSMF-DCF model has been used with total transmission distance of 2030 km and input power of 1 mW. At 20% and 40% duty cycles of RZ pulse, pulse center varies 5.1527 ps and 5.1442 ps respectively. However, at higher duty cycle i.e. when D is more than 50%, these variations become comparatively less as pulse width is more, so TOD effect will be comparatively less . Fig. 5.6 shows that for D = 60% and 80%, pulse center shifts 4.8231 ps and 4.2444 ps respectively for 2030 km variation of distance.

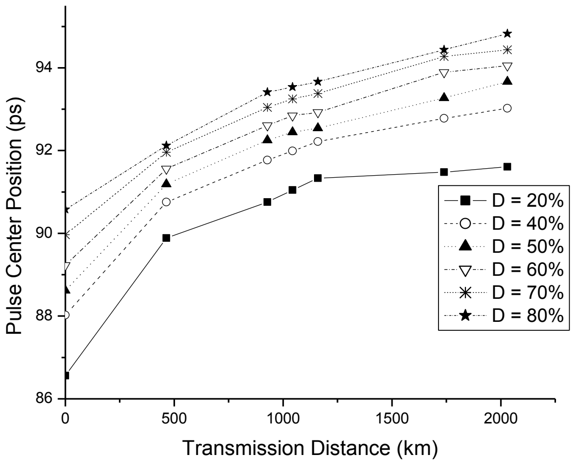

Figure 5.6: Variation of pulse center position with transmission distance varying duty cycle (D) of 100 Gb/s RZ Gaussian pulse.

Fig.5.7 depicts clearly the temporal shift of RZ Gaussian pulse center position with D for transmission reach of 2030 km. Here, it is observed that the shifting reduces with the increase of D for a particular bit rate. This can be explained using a simple example. For example, if bit rate = B, Filter width = F_w, Duty cycle = D, then

$$\text{Symbol rate, } S_r = \frac{B}{F_w} \qquad (5.1)$$

$$\text{Time slot, } T_s = \frac{1}{S_r} = \frac{F_w}{B} \qquad (5.2)$$

$$\text{FWHM time, } T_{FWHM} = T_s \times D = \frac{F_w}{B} \times D \qquad (5.3)$$

$$\text{Initial Gaussian pulse width, } T = \frac{T_{FWHM}}{1.665} = \frac{F_w}{1.665 \times B} \times D \qquad (5.4)$$

From equation (5.4), we can say that initial pulse width is proportional to the duty cycle. As a result, with the increase of duty cycle pulse width increases as a result TOD effect is relatively less which in turn reduces the temporal shift of RZ Gaussian pulse.

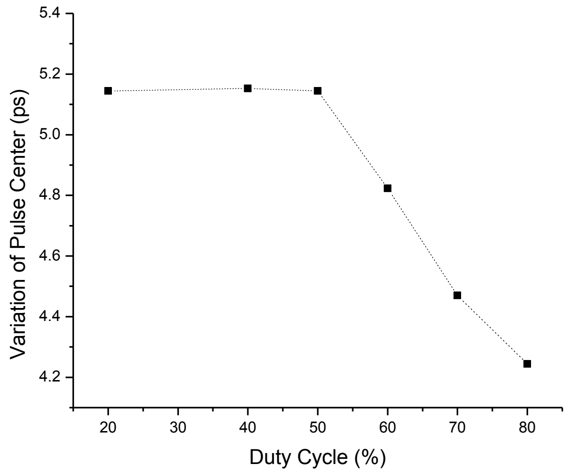

Figure 5.7: Variation of pulse center with varying duty cycle (D) for 100 Gb/s RZ Gaussian pulse.

5.3.3 Changes of Pulse Center Position for Different Fiber Types

Again, pulse center position also varies with the propagation of different types of pulses and fibers for same bit rate. Fig. 5.8 depicts these variations.

In the next simulation, different types of fibers have been utilized to observe the time shifting of pulse center position of received pulse due to impact of TOD for 100 Gb/s

Rz Gaussian pulse. When NZDSF-DCF is used, variation of pulse center position is comparatively lower than that of SSMF-DCF as shown in fig. 5.8.

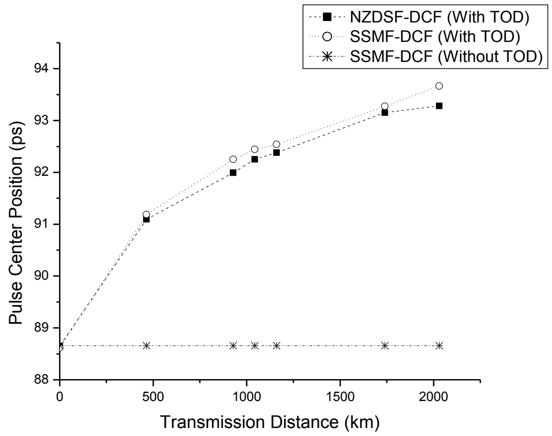

Figure 5.8: Pulse center position versus propagation distance for different fiber types of 100Gb/s.

5.4 TOD Compensation

When the bit rate of a single channel exceeds 100 Gb/s, one must use ultrashort pulses (width ~ 1 ps) in each bit slot. For such short optical pulses, the pulse spectrum becomes broad enough that it is difficult to compensate GVD over the entire bandwidth of the pulse (because of the frequency dependence of β_2). The simplest solution to this problem is provided by fibers, or other devices, designed such that both β_2 and β_3 are compensated simultaneously. However, for a 1-ps pulse, it is sufficient to satisfy Eq. ($\beta_{21}L_1 + \beta_{22}L_2 = 0$) over a 4–5 nm bandwidth. This requirement is easily met for DCFs, especially designed with negative values of β_3 (sometimes called reverse-dispersion fibers). In this report, we have used DCF and FBG for compensating the GVD and TOD effects.

5.4.1 Dispersion Compensation using DCF

In our simulation, we have used two models for dispersion-managed (DM) transmission systems. One model consists of SSMF and DCF. In another model, NZDSF is followed by DCF. Fig. 5.9 shows the schematic diagram of SSMF-DCF model.

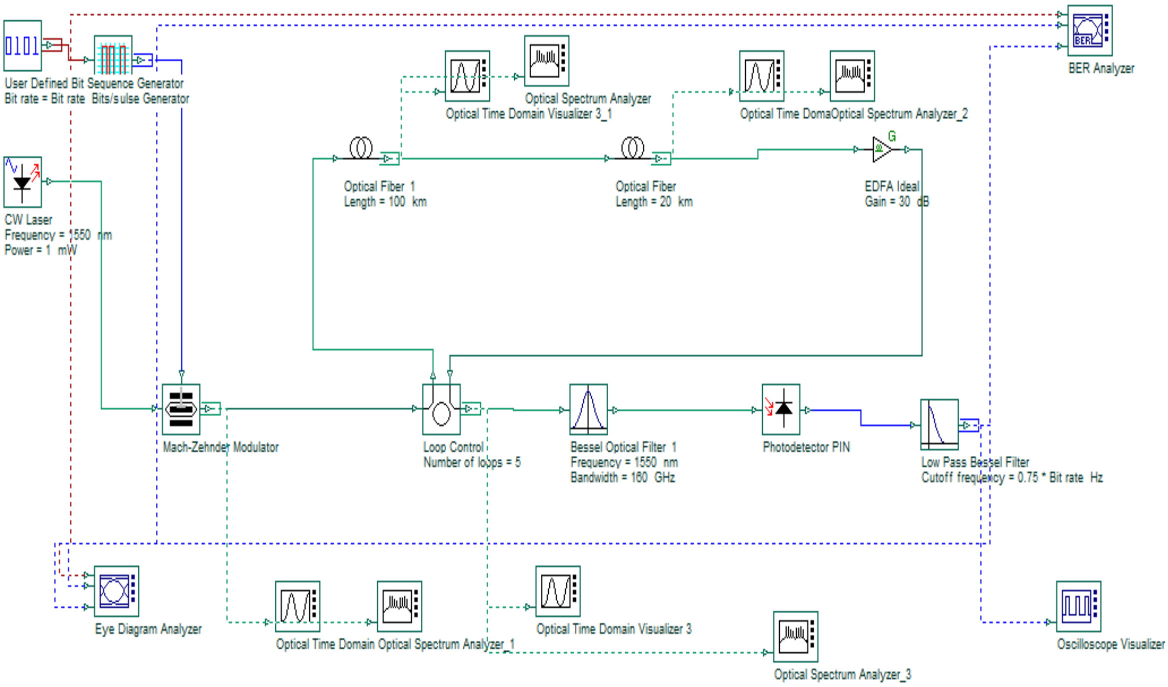

Figure 5.9: Schematic diagram of SSMF-DCF dispersion-managed transmission system.

The following fiber parameters are given for the simulation process:

Table 12: Simulation Parameters of SSMF-DCF

Parameters	**SSMF**	**DCF**
Reference wavelength, λ (nm)	1550	1550
Length, L (km)	50	8
Attenuation, α_{dB} (dB/km)	0.2	0.5
Dispersion, D (ps/nm-km)	16	-100
Dispersion slope, S (ps/nm^2-km)	0.08	0.08
Differential group delay (ps/km)	0.2	0.2
Effective area, A_{eff} (um^2)	80	23
Nonlinear refractive index, n_2 (m^2/W)	2.6e-020	3e-020

Simulation results for 40, 100, 160 and 320 Gb/s are given below-

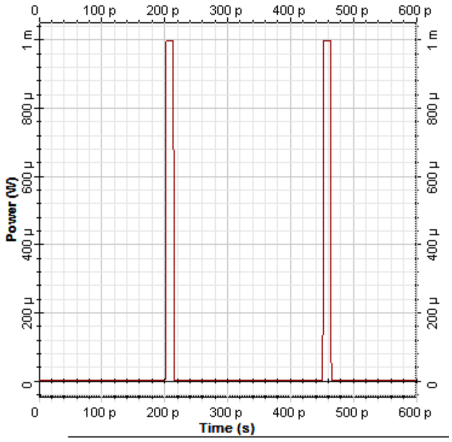

(a)

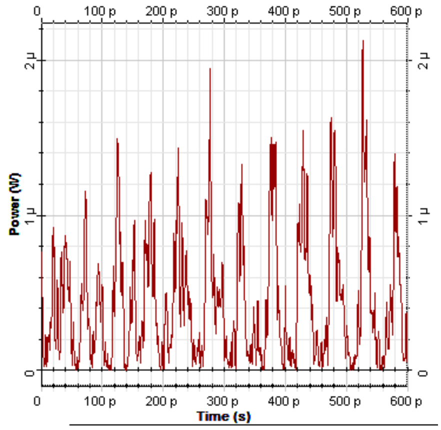

(b)

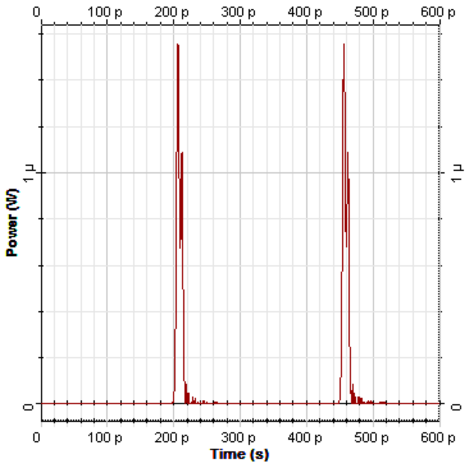

(e)

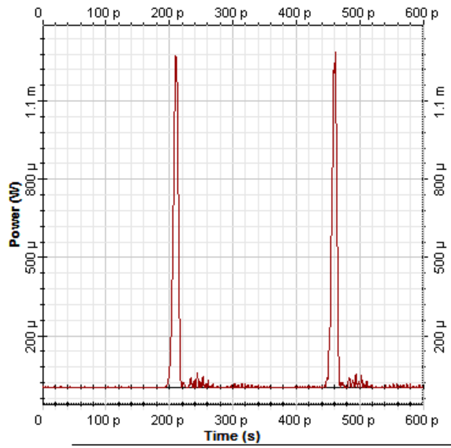

(f)

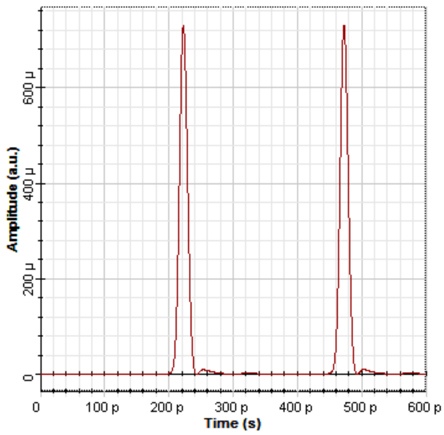

(g)

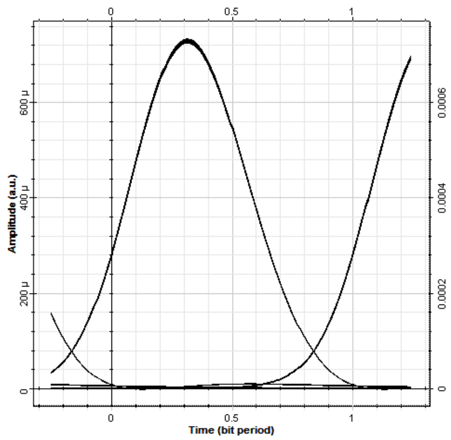

(h)

Figure-5.10: Output waveforms at different stages for B = 40Gb/s, duty cycle = 50%, propagation distance = 1218 km - (a) input pulse, (b) After SSMF, (c) After DCF, (d) After amplifier, (e) after electric filter at the receiver end and (f) Eye diagram at the receiver end (Q = 207.725, BER = 0).

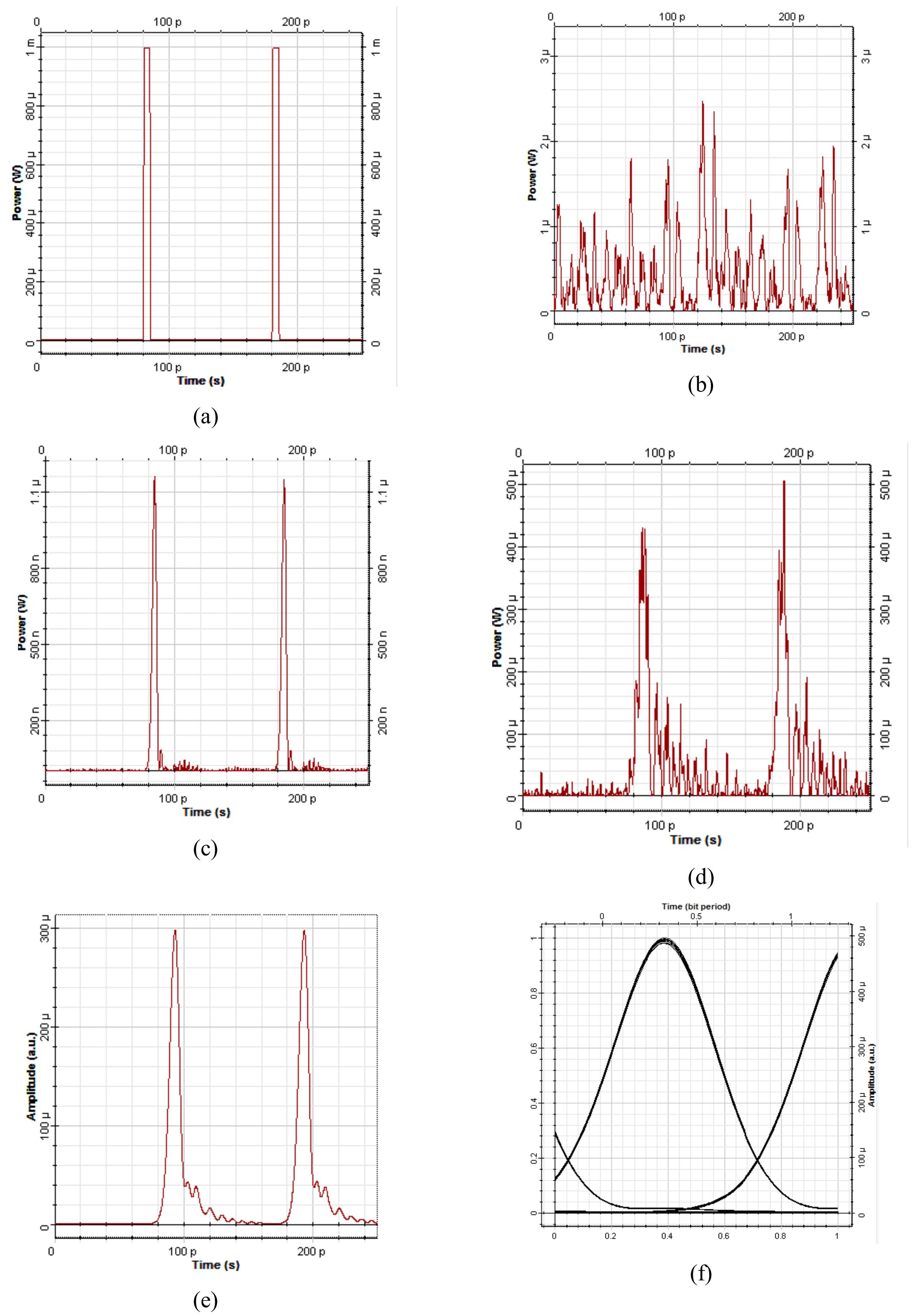

Figure-5.11: Output waveforms at different stages for B = 100 Gb/s, duty cycle = 50%, propagation distance = 1218 km - (a) input pulse, (b) After SSMF, (c) After DCF, (d) After amplifier, (e) after electric filter at the receiver end and (f) Eye diagram at the receiver end (Q = 17. 4152, BER = 3.06×10^{-68}).

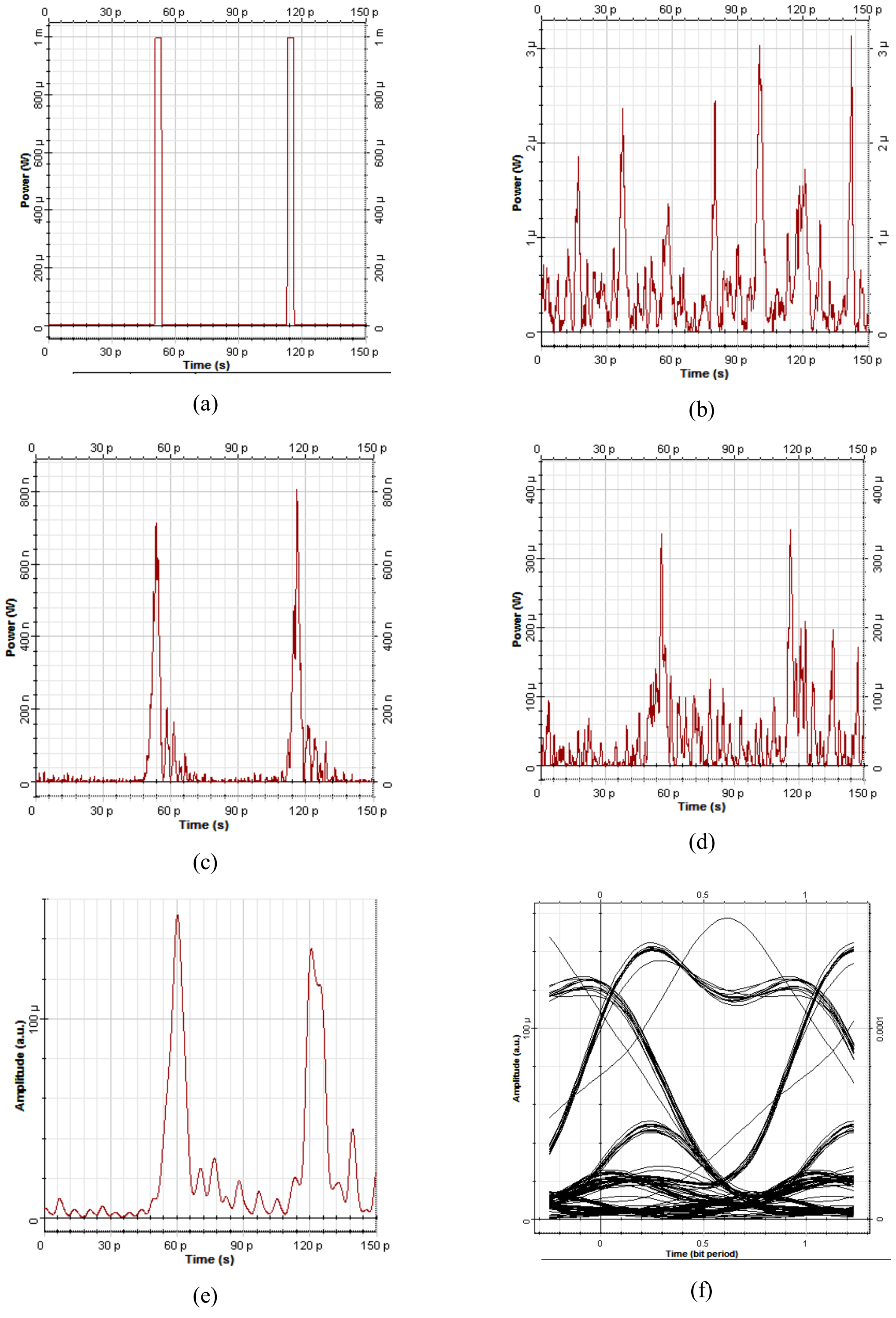

Figure-5.12: Output waveforms at different stages for B = 160Gb/s, duty cycle = 50%, propagation distance = 1218 km - (a) input pulse, (b) After SSMF, (c) After DCF, (d) After amplifier, (e) after electric filter at the receiver end and (f) Eye diagram at the receiver end (Q = 6.92636, BER = 2.316×10^{-12}).

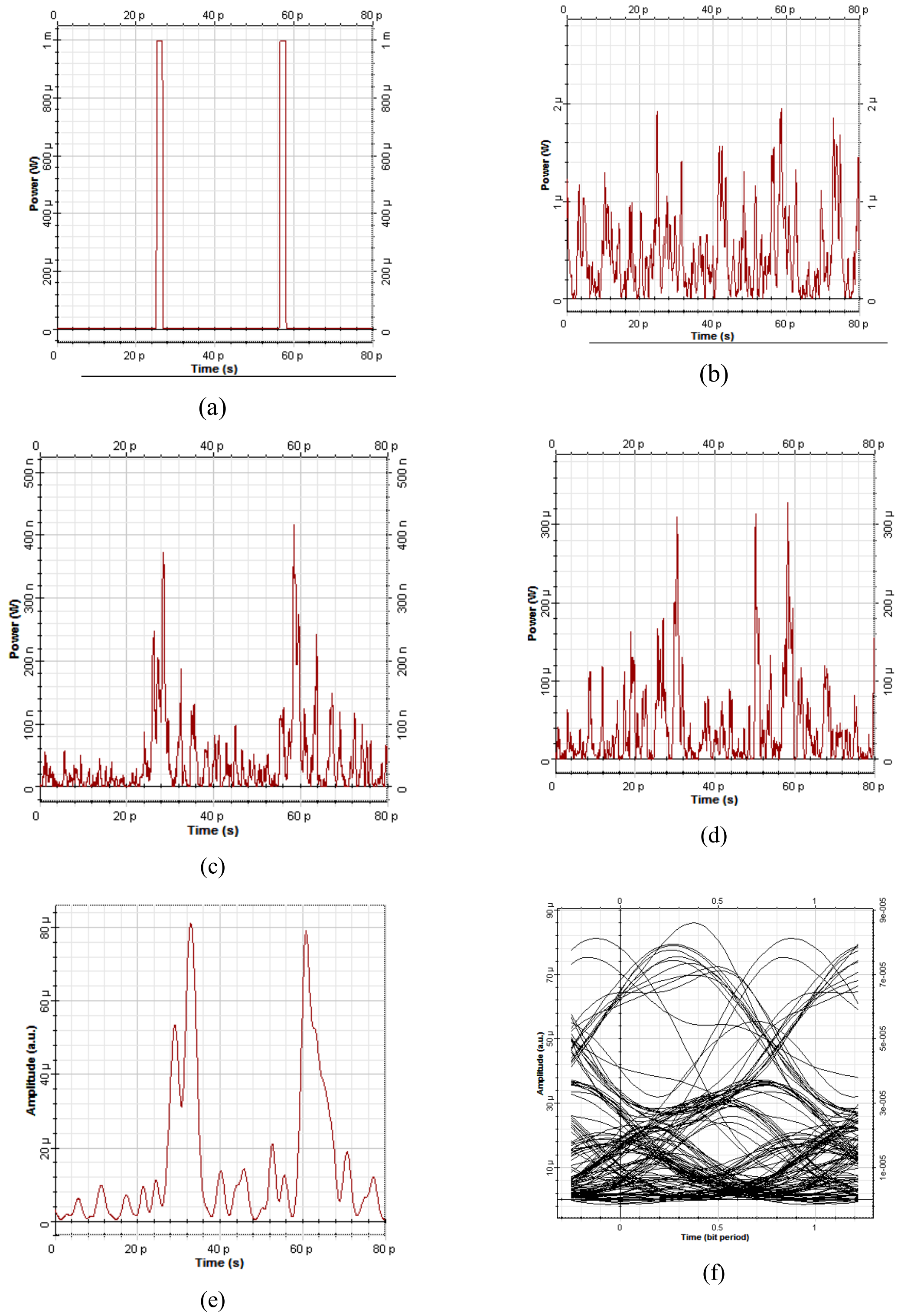

Figure-5.13: Output waveforms at different stages for B = 320 Gb/s, duty cycle = 50%, propagation distance = 1218 km - (a) input pulse, (b) After SSMF, (c) After DCF, (d) After amplifier, (e) after electric filter at the receiver end and (f) Eye diagram at the receiver end (Q = 2.82599, BER = 1.927×10^{-3}).

From the above figures (5.10 to 5.13), we can say that as the bit rate increases both second order and third order dispersion dominant. Second order dispersion effect can be easily compensated using DCF. But DCF cannot minimize the TOD effects, as a result some ripples still present in the electrically filtered output waveforms. Again, values of Q and BER degrade with the increase of data rate. High Q factor shows that the signal is less immune to noise and received signal is similar to input signal with less noise.

Our second model consists of NZDSF and DCF. Schematic diagram using OptiSystem is shown in fig. 5.14.

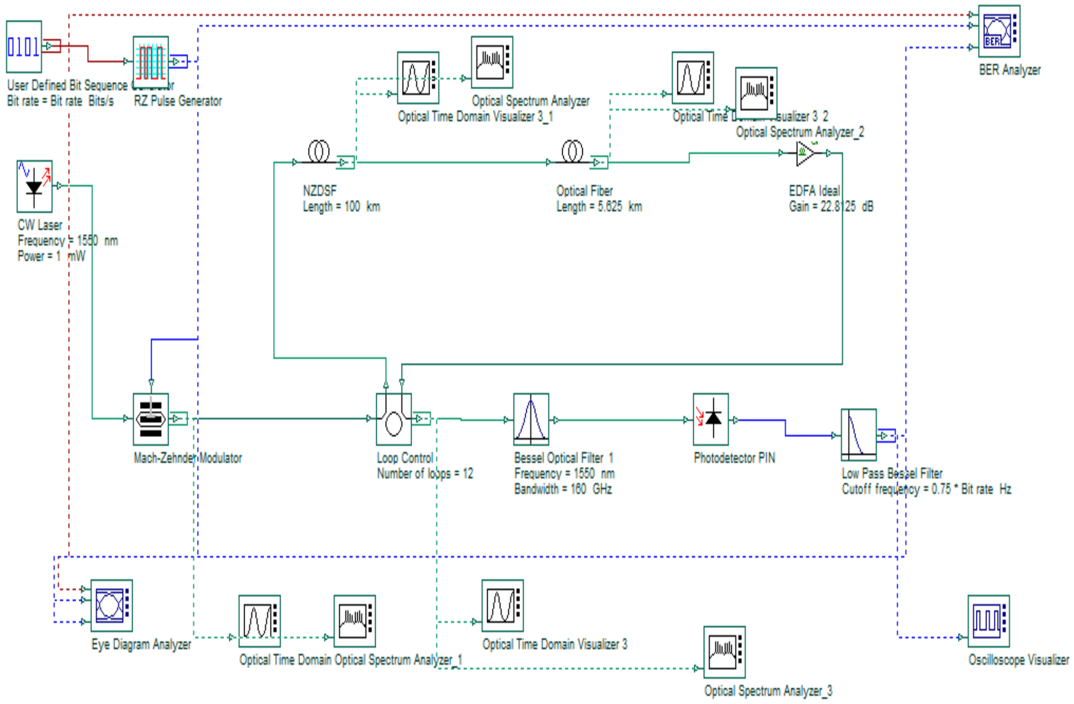

Figure 5.14: Schematic diagram of NZDSF-DCF dispersion-managed transmission system.

The following fiber parameters are given for the simulation process:

Table 13: Simulation Parameters of NZDSF-DCF

Parameters	**NZDSF**	**DCF**
Reference wavelength, λ (nm)	1550	1550
Length, L (km)	57.5	2.5
Attenuation, α_{dB} (dB/km)	0.2	0.5
Dispersion, D (ps/nm-km)	4.5	-100
Dispersion slope, S (ps/nm^2-km)	0.07	0.08
Differential group delay (ps/km)	0.2	0.2
Effective area, A_{eff} (um^2)	70	23
Nonlinear refractive index, n_2 (m^2/W)	2.6e-020	3e-020

Simulation results for 40, 100, 160 and 320 Gb/s are given below-

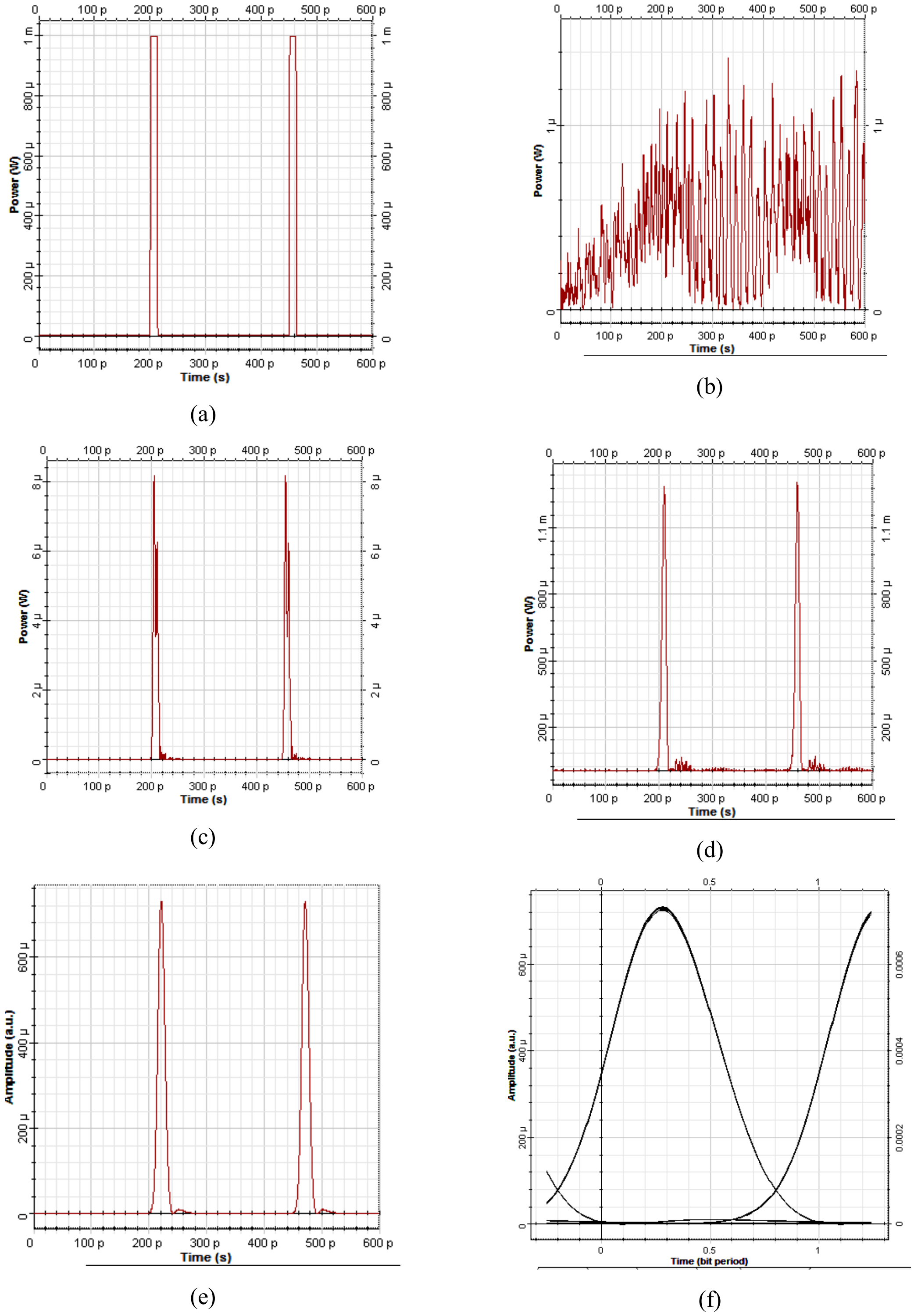

Figure-5.15: Output waveforms at different stages for B = 40Gb/s, duty cycle = 50%, propagation distance = 1218 km- (a) input pulse, (b) After NZDSF, (c) After DCF, (d) After amplifier, (e) after electric filter at the receiver end and (f) Eye diagram at the receiver end (Q =198.937, BER =0)

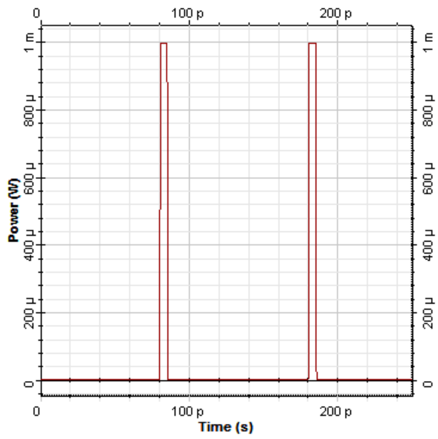

(a)

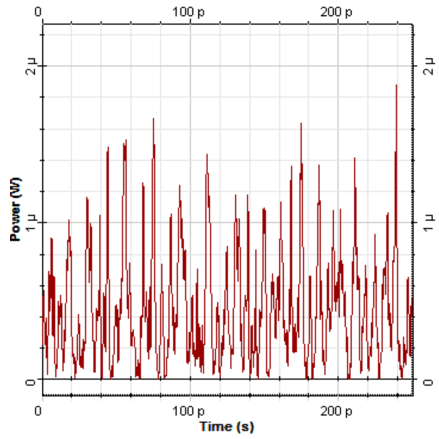

(b)

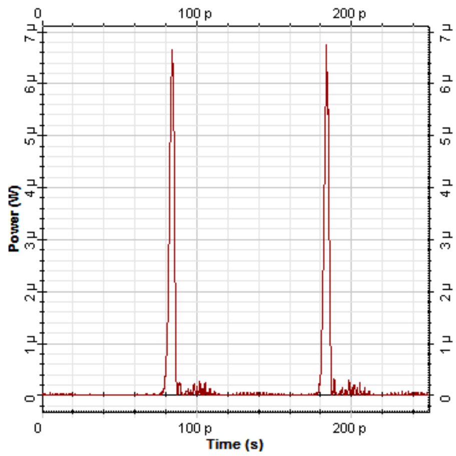

(c)

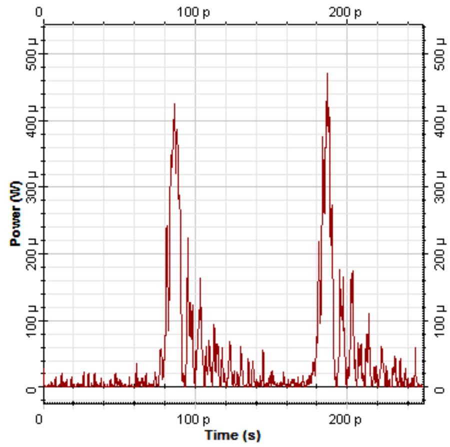

(d)

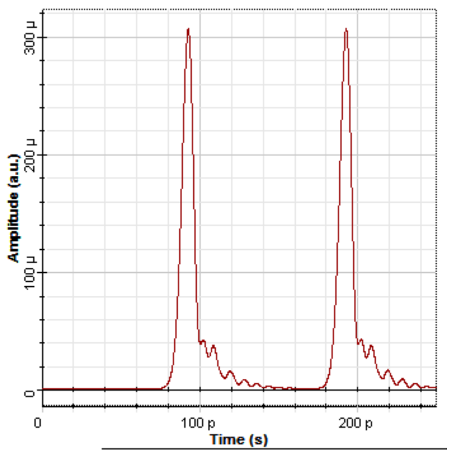

(e)

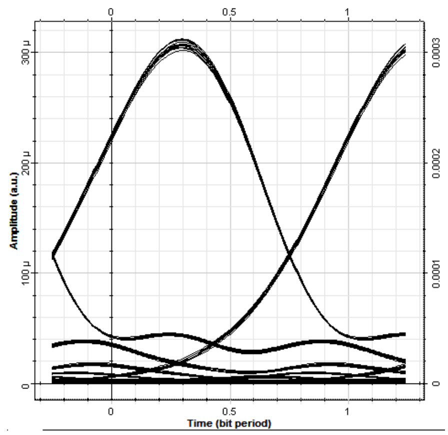

(f)

Figure-5.16: Output waveforms at different stages for B = 100Gb/s, duty cycle = 50%, propagation distance = 1218 km- (a) input pulse, (b) After NZDSF, (c) After DCF, (d) After amplifier, (e) after electric filter at the receiver end and (f) Eye diagram at the receiver end (Q =18.5383, BER =4.859×10^{-77})

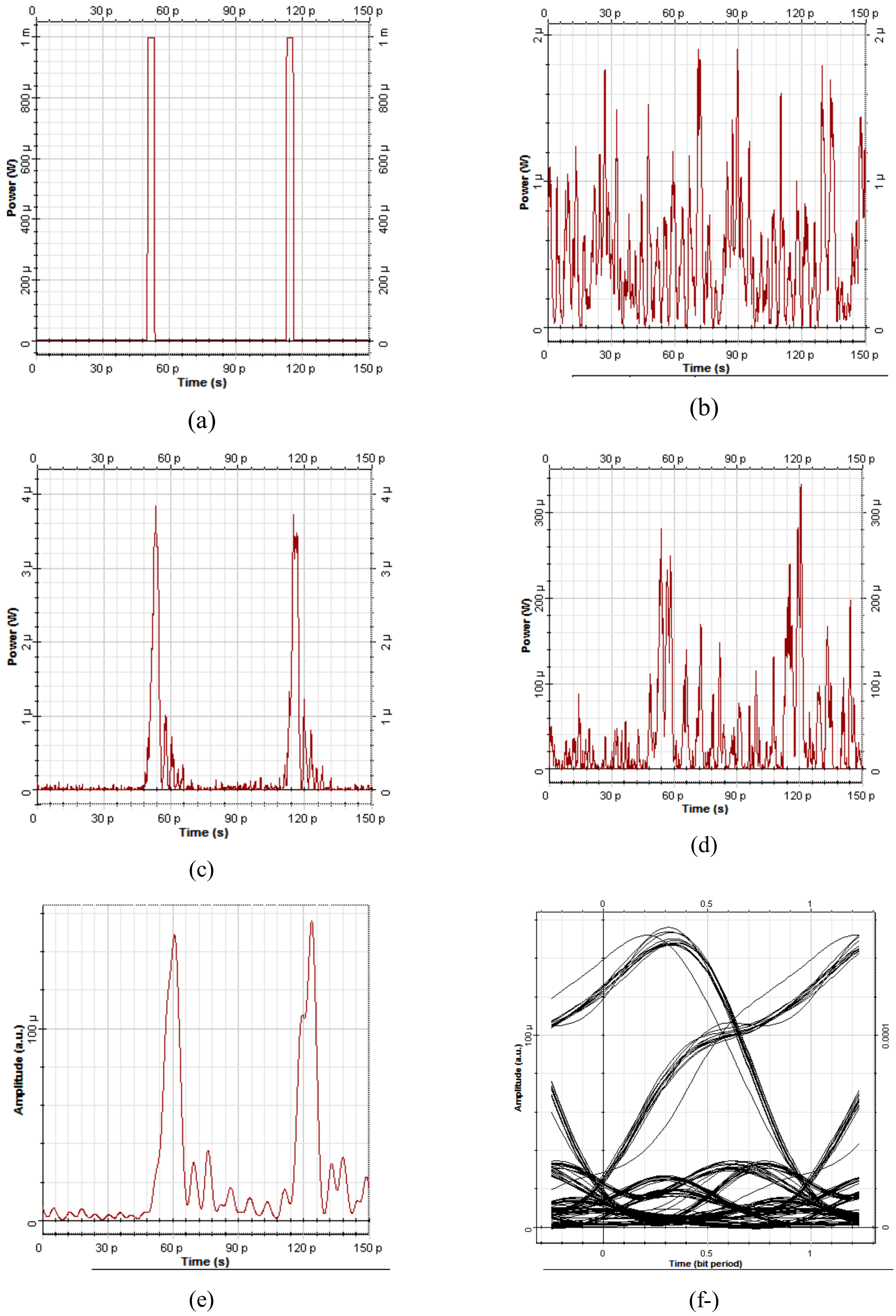

(a) (b) (c) (d) (e) (f-)

Figure-5.17: Output waveforms at different stages for B = 160 Gb/s, duty cycle = 50%, propagation distance = 1218 km- (a) input pulse, (b) After NZDSF, (c) After DCF, (d) After amplifier, (e) after electric filter at the receiver end and (f) Eye diagram at the receiver end (Q =9.244, BER =8.75×10^{-21}).

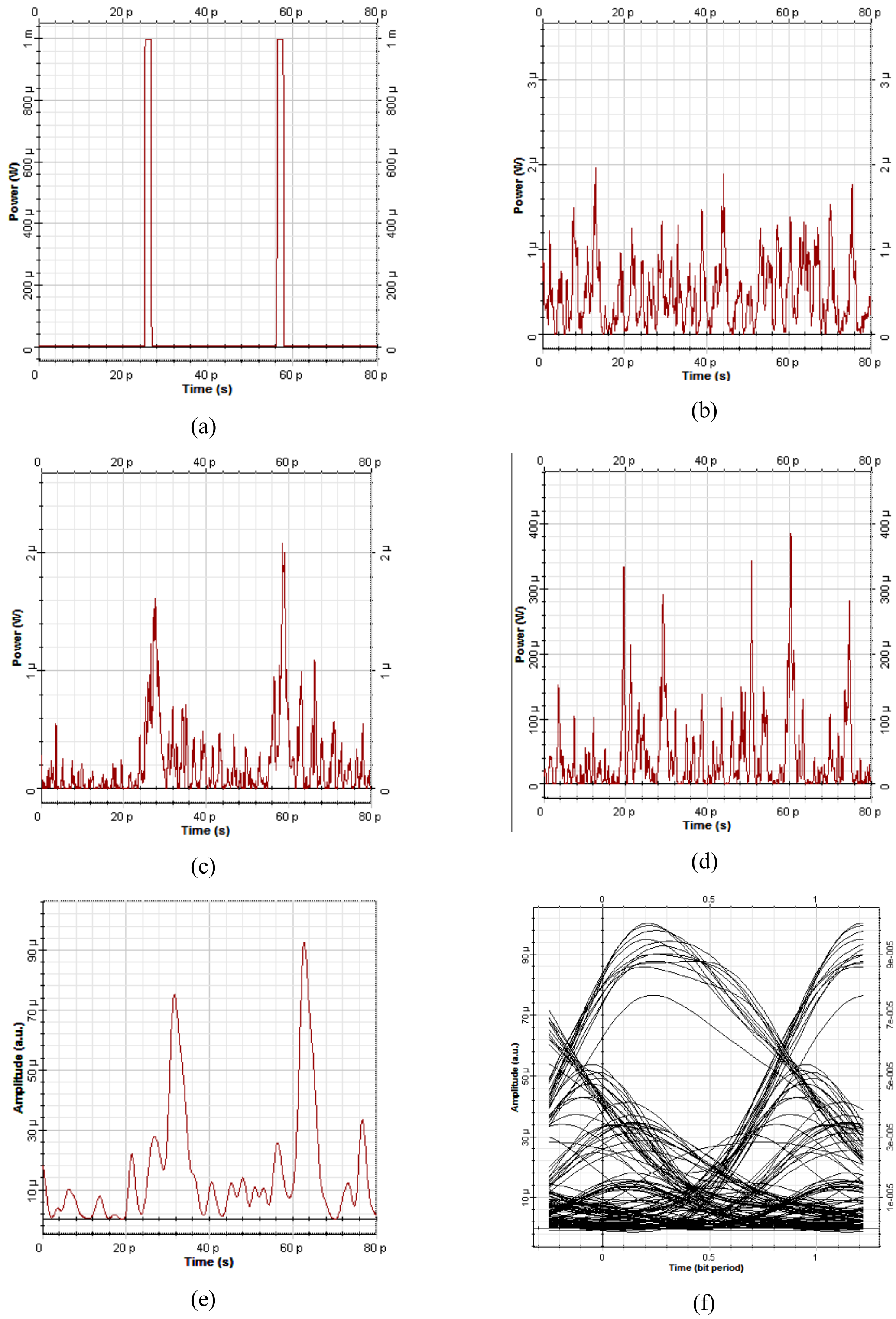

Figure-5.18: Output waveforms at different stages for B = 320Gb/s, duty cycle = 50%, propagation distance = 870km(a) input pulse, (b) After NZDSF, (c) After DCF, (d) After amplifier, (e) after electric filter at the receiver end and (f) Eye diagram at the receiver end (Q =6.12042, BER =3.061×10^{-10}).

From the above figures (5.14 to 5.18), we can say that as the bit rate increases both second order and third order dispersion dominant. Second order dispersion effect can be easily compensated using DCF. But DCF cannot minimize the TOD effects, as a result some ripples still present in the electrically filtered output waveforms. Again, values of Q and BER degrade with the increase of data rate. High Q factor shows that the signal is less immune to noise and received signal is similar to input signal with less noise.

5.4.2 TOD Compensation using FBG

Second order dispersion can be compensated using DCF. But it cannot compensate TOD. So, FBG has been used to compensate TOD effect. In our simulation, we have used SSMF which is followed by FBG. Schematic diagram of SSMF-FBG transmission system is shown in fig. 5.19.

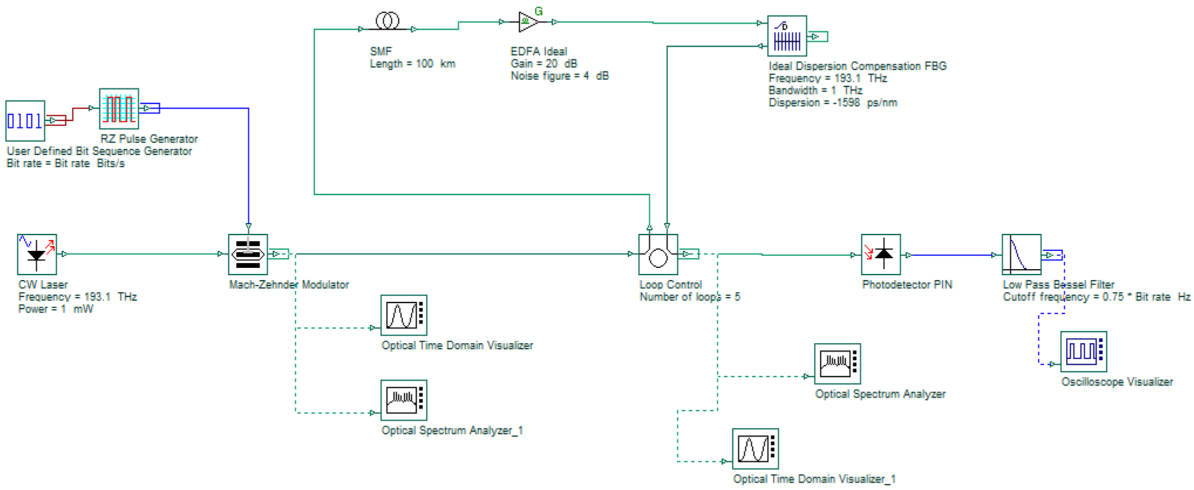

Figure 5.19: Schematic diagram of SSMF-FBG dispersion-managed transmission system.

The following fiber parameters are given for the simulation process:

Table 14: Simulation Parameters of SSMF-FBG

Parameters	**SSMF**
Reference wavelength, λ (nm)	1550
Length, L (km)	100
Attenuation, α_{dB} (dB/km)	0.2
Dispersion, D (ps/nm-km)	16
Dispersion slope, S (ps/nm^2-km)	0.08
Differential group delay (ps/km)	0.2
Effective area, A_{eff} (um^2)	80
Nonlinear refractive index, n_2 (m^2/W)	2.6e-020

Parameters	FBG
Frequency (THz)	193.1
Bandwidth (THz)	1
Insertion loss (dB)	0
Depth (dB)	100
Dispersion (ps/nm)	-1598 ~ 1605

Simulation results for 40, 100, 160 and 320 Gb/s are given below-

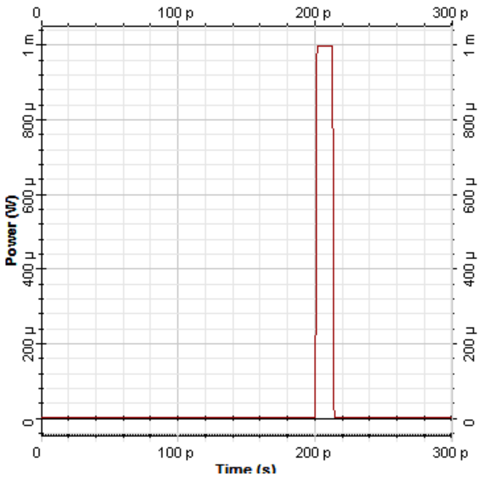

(a)

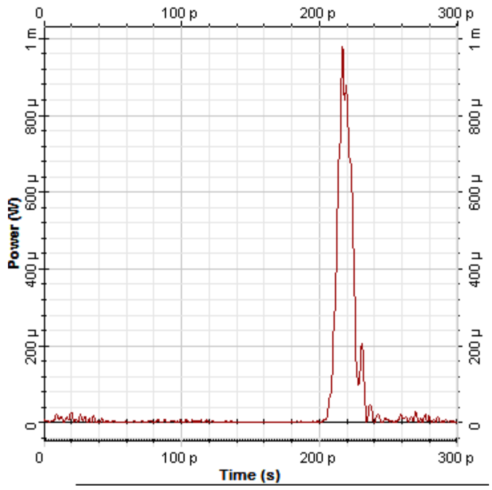

(b)

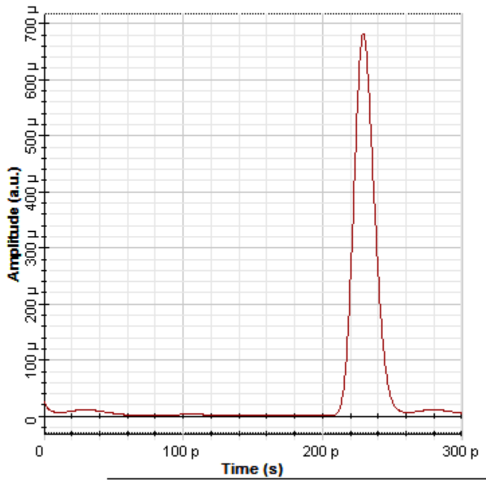

(c)

Figure-5.20: Output waveforms at different stages for B = 40Gb/s, duty cycle = 50%, propagation distance = 1000km- (a) input pulse, (b) After amplifier, (c) after electric filter at the receiver end.

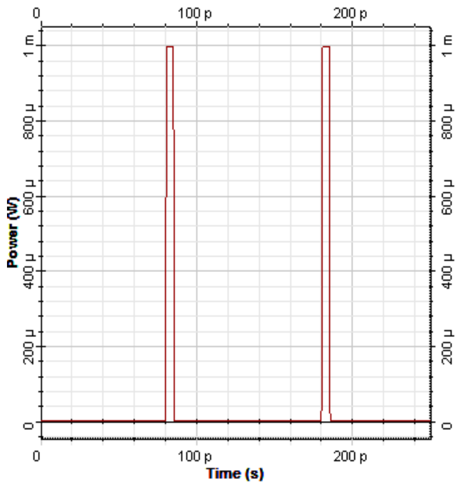

(a)

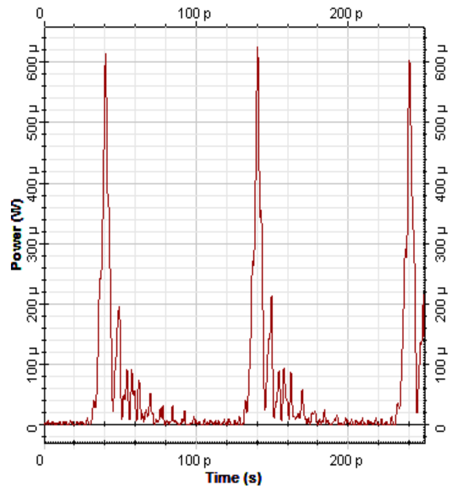

(b)

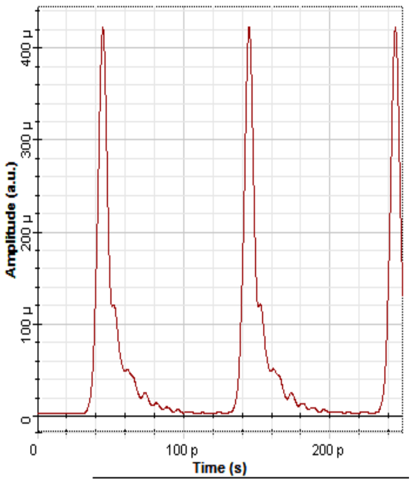

(c)

Figure-5.21: Output waveforms at different stages for B = 100 Gb/s, duty cycle = 50%, propagation distance = 600km- (a) input pulse, (b) After amplifier, (c) after electric filter at the receiver end.

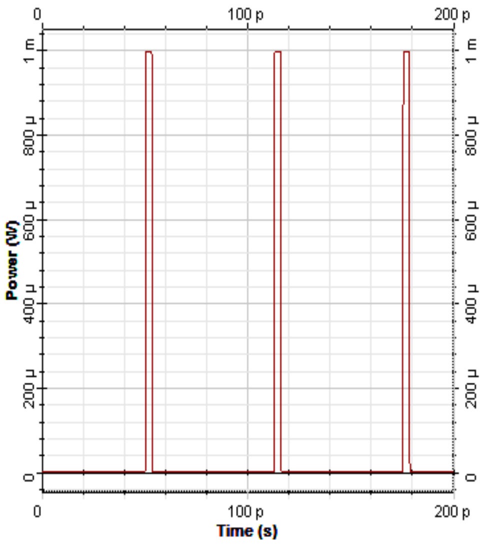

(a)

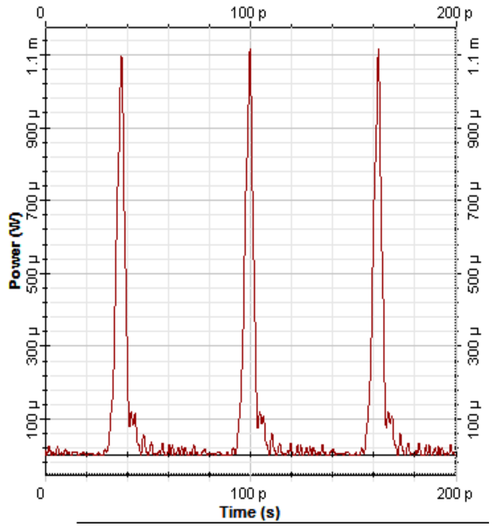

(b)

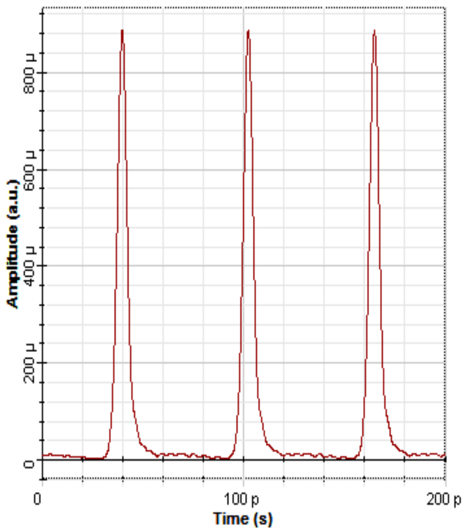

(c)

Figure-5.22: Output waveforms at different stages for B = 160 Gb/s, duty cycle = 50%, propagation distance = 300km- (a) input pulse, (b) After amplifier, (c) after electric filter at the receiver end.

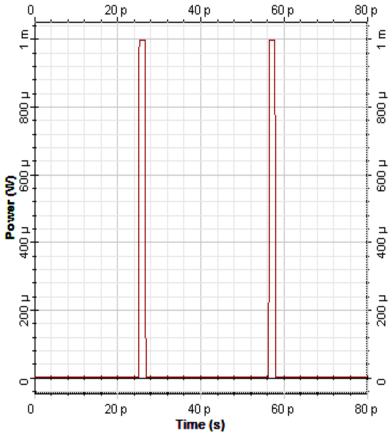

(a)

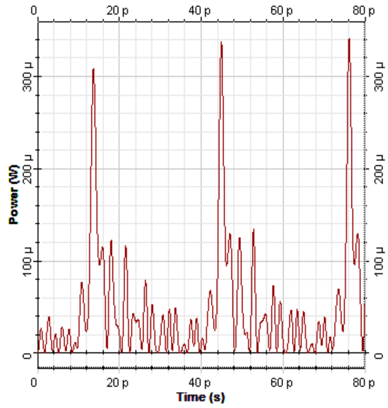

(b)

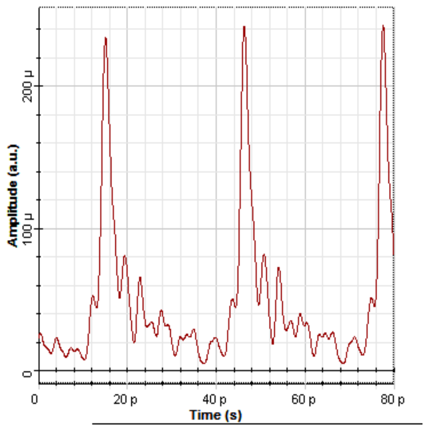

(c)

Figure-5.23: Output waveforms at different stages for B = 320 Gb/s, duty cycle = 50%, propagation distance = 100km- (a) input pulse, (b) After amplifier, (c) after electric filter at the receiver end.

From the above figures (5.20 to 5.23), it can be said that TOD can be compensated using FBG. FBGs have a negligible nonlinearity, low insertion loss and small size. The in line dispersion is compensated using a real grating component for a 100 km fiber. The results are validated by comparing the Q factor of the FBG simulated model for before compensation and after compensation. The simulation results are shown in Table.15.

Table 15: Simulation Results for the FBG dispersion compensation for PIN receiver

FBG for pin receiver	**Before Compensation (Only SSMF, d = 0.5km)**	**After Compensation (SSMF-FBG, d = 100km)**
Q factor (dB)	2.87371	4.67556
BER	2.01625×10^{-3}	4.33387×10^{-7}

5.5 Conclusion

TOD effect is evaluated by varying bit rates, transmission distances, duty cycles, pulse shapes and different transmission models for dispersion-managed system using OptiSystem. Temporal shift effect of TOD increases with the increment of transmission distances and bit rates and decreases with the increase of duty cycle for a particular DM system. SSMF-DCF system can compensate only GVD. SSMF-FBG system can compensate both GVD and TOD for ultra high speed optical fiber communication system.

Chapter Six

Conclusion

6.1 Summary

This thesis dealt with analysis of TOD effect on ultra-high bit rates in optical fiber system. TOD effects have disadvantages in the form of limiting the transmission rate of transmitted signal in the system. Initially, the theoretical analysis and comparison of TOD effects has been presented and then the effects has been practically compared with the theoretical analysis of TOD effects by simulating the design models in OptiSystem tool and compared these effects against each other with respect to Q factor. Later on, short modeling of numerical analysis of nonlinear Schrödinger equation using Split step algorithm is done to analyze the effects of nonlinearity in fiber, which is coded and optimized in Matlab. TOD effect is evaluated by varying bit rates, transmission distances, duty cycles, pulse shapes and different transmission models for dispersion-managed system using the simulations in OptiSystem.

Chapter two provides a brief description about the impact of different transmission impairments of optical fiber communication system. Linear impairments such as attenuation and fiber dispersion are discussed here. Also different types of nonlinear impairments such as SPM, XPM, SBS, SRS and FWM are explained in this chapter.

The fundamental equation for optical pulse propagation in a fiber has been introduced considering a Gaussian solution of NLS equation in chapter three. Analytical calculation of pulse broadening and changes of pulse shapes due to GVD and TOD on RZ Gaussian pulse have been explained. Then we used the numerical method, SSFM to check the results observed by the analytic technique. Both this techniques are described in this chapter for dispersion management system.

The simulation model using OptiSystem has been presented in chapter four. Dispersion compensated system model has three parts- transmission section, optical link section and receiver section. Components of the each section were also conferred in this chapter.

Simulation results are discussed in chapter five. First, the specification of the different models used for our simulations have been discussed. Then the analytic and numerical plots are given for these models with respect to different parameters. Two different models are used to explore the TOD effect for different high bit rate systems, duty cycle, dispersion map strength and fiber types for dispersion managed transmission system. One model consists of SSMF and DCF. In another model, NZDSF is followed by DCF. We have also observed the time-shift without and with TOD. The TOD compensation technique using fiber Bragg's grating for ultra-high speed optical communication system was also used.

From the results obtained, it can be concluded that the presence of the TOD causes pulse expansion as well as introduces an additional temporal shift to each pulse. Oscillatory tail due to TOD might be a major limiting factor in the way to realize long-haul high speed transmission systems. With the increase of bit rate, temporal shift of pulse center increases. Pulse center position also changes with the variation of duty cycles, pulse shapes and fiber types. However, these impairments could be mitigated by properly designing DM transmission systems along with consideration of other parameters. As far as real environment is considered, performance of RZ Gaussian pulse using SSMF-DCF system is better than NZDSF-DCF for ultra-high speed if both GVD and TOD effects are considered. But SSMF-DCF system cannot completely diminish the TOD effects. Performance of SSMF-FBG is satisfactory while considering both GVD and TOD for high bit rate.

6.2 Future work

In this thesis we have investigated optical pulse propagation in dispersion managed system. Only self-phase modulation, second and third order dispersion effects, fiber loss, ASE noise and receiver noises are considered here. So this investigation needs further modification by considering other nonlinear effects. Again, we have only considered single channel fiber transmission and dispersion management system. Corresponding transmitter and receiver and other supporting devices should be designed accordingly with this kind of dispersion managed system which we did not study in this thesis. So there are a lot of investigations yet to be done in this area. Further optimization of the designs can be achieved for higher bit rates such as 320 Gb/s or more.

With increasing bit rate, TOD effect is going to be more dominant in transmission line and contributing error along with the other errors. So, the TOD effect must be investigated for these high speed lines and also for different kinds of modulation formats (DPSK, DQPSK, QPSK etc.). All the designs were not physically implemented (using hardware) due to insufficient resources. In future, physically implementation can be done and compare the results of simulations with the results of physical implementation.

Bibliography

[1] G. J. Holzmann and B. Pehrson, "The early history of data networks", *IEEE Computer Society Press,* Los Alamitos, CA, 1995.

[2] G. P. Agrawal, Fiber-optic communication systems, 3rd edition, *John Wiley,* 2002.

[3] S. Kawanishi, H. Takara, O. Kamatani, T. Morioka, and M. Saruwatari, "100 Gbit/s, 560 km optical transmission experiment with 80 km amplifier spacing employing dispersion management", *Electron. Lett.*, vol. 32, pp. 470 -471, 1996.

[4] S. Kawanishi, H. Takara, T. Morioka, O. Kamatani, K. Takiguchi, T. Kitoh, and M. Saruwatari, "Single channel 400 Gbit/s time-division-multiplexed transmission of 0.98 ps pulses over 40 km employing dispersion slope compensation", *Electron. Lett.*, vol. 32, pp. 916 -918, 1996.

[5] K. Takiguchi, S. Kawanishi, H. Takara, O. Kamatani, K. Uchiyama, A. Himeno, and K. Jinguji, "Dispersion slope equalizing experiment using planar lightwave circuit for 200 Gbit/s time-division-multiplexed transmission", *Electron. Lett.*, vol. 32, pp. 2083 -2084, 1996.

[6] C. C. Chang and A. M. Weiner, "Fiber transmission for sub-500-fs pulses using a dispersion-compensating fiber", *IEEE J. Quantum Electron.*, vol. 33, pp. 1455 - 1464, 1997.

[7] S. Shen and A. M. Weiner, "Complete dispersion compensation for 400-fs pulse transmission over 10-km fiber link using dispersion compensating fiber and spectral phase equalizer", *IEEE Photon. Technol. Lett.,* vol. 11, pp. 827, 1999.

[8] J. Kwon, S. Kim, S. Roh and B. Lee, "Tunable dispersion slope compensator using a chirped fiber bragg grating tuned by a fan-shaped thin metallic heat channel", *IEEE Photon. Technol. Lett.*, vol. 18, no. 1, pp. 118–120, 2006.

[9] G. P. Agrawal, Nonlinear Fiber Optics, 3rd edition, *Academic Press,* 2001.

[10] N. Cheng and J. C. Cartledge, "Power penalty due to the amplitude and phase response ripple of a dispersion compensating fiber bragg grating for chirped optical signals*", IEEE J. of Lightwave Technol.*, vol. 24, no. 9, pp. 3363–3369, 2006.

[11] N. S. Bergano, and C. R. Davidson "Wavelength division multiplexing in long haul transmission systems", *IEEE J. of Lightwave Technol.*, vol. 14, pp. 1299-

1308, 1996.

[12] E. Forestieri and G. Prati: "Novel optical line codes tolerant to fiber chromatic dispersion", *IEEE J. of Lightwave Technol.,* vol. 19, no. 11, 2001.

[13] J. Lively, "Dealing with the critical problem of chromatic dispersion", *Lightwave*, 1998.

[14] B. Jopson and A. Gnauck, "Dispersion compensation for optical fiber systems", *IEEE Commun. Mag.,* vol. 33, pp. 96–102, June 1995.

[15] K. Takiguchi, S. Kawanishi, H. Takara and A. Himeno ,"Dispersion slope equalizer for dispersion shifted fiber using a lattice-form programmable optical filter on a planar lightwave circuit", *IEEE J. of Lightwave Technol*. vol. 16, pp. 1647-1657, 1998.

[16] M. I. Hayee and A. E. Willner, "NRZ versus RZ on 10-40 Gb/s dispersion managed WDM transmission systems", *IEEE Photon. Technol. Lett*. vol. 11, pp. 991, 1999.

[17] H. Tsuda, K. Yokomato, T. Ishii, T. Kurukawa, H. Takenouchi and Y. Inoue, "Second- and third-order dispersion compensator using a high-resolution arrayed-waveguide grating", *IEEE Photon. Technol. Lett.,* vol. 5, no. 11, pp. 569-571, May 1999.

[18] C. H. Kim, J. Bae, K. Lee and S. B. Lee, "Performance evaluation of strain chirped fiber bragg grating based tunable dispersion compensator with 40 Gb/s signal", *In: Proceedings of Opto-Electronics and Communications Conference (OECC),* 2008.

[19] X. Tang, N. Y. Kim, S. Doucet, S. La Rochelle and J. C. Cartledge, "Impact of phase ripple in fiber bragg grating based tunable dispersion compensator on 10 Gb/s NRZ transmission", *In: Proceedings of Optical Fiber Communication and the National Fiber Optic Engineers Conference (OFC/NFOEC)*, 2007.

[20] T. Komukai and T. Inui, "The design of dispersion equalizers using chirped fiber bragg gratings", *IEEE J. Quantum Electronics,* vol. 36, no. 6, pp. 409-416, 2000.

[21] M. Ibsen and R. Feced, "Fiber Bragg gratings for pure dispersion-slope compensation," *Opt. Lett.*, vol. 28, pp. 980, 2003.

[22] X. Wang, K. Kikuchi and Y. Takushima, "Analysis of dispersion-managed optical fiber transmission system using NRZ pulse format and performance restriction from third-order dispersion", *IEICE trans. Electron*, vol. E82-C, no. 8,

pp. 1407-1413, August, 1999.

[23] H. Taga, "Long distance transmission experiments using the WDM technology", *J. Lightwave Technol*., vol. 14, pp. 1287, 1996.

[24] D. Marcuse, "Pulse distortion in single-mode fibers", *Appl. Opt.* vol. 19, pp. 1653, 1980.

[25] G. P. Agrawal and M. J. Potasek, "Effect of frequency chirping on the performance of optical communication systems", *Opt. Lett. ,* vol. 11, pp. 318, 1986.

[26] M. Miyagi and S. Nishida, "Pulse spreading in a single-mode fibre due to third-order dispersion", *Appl. Opt.,* vol. 18, no. 5, pp. 678-682, 1979.

Appendix

```
% Program to simulate propagation of SMF + DCF, no fiber loss and without TOD
clear all;
close all;
niter=10;       % value set to save the pulse data
gamma1 = 1.2667;
gamma2 = 6.40053;
gvd1 = -21.6676;
gvd2 = +127.4566;
%%%%%Fiber
L1 = 43; % anomalous dispersion length of the fiber
L2 = 7.31; % normal dispersion length of the fiber
ave_gvd=(gvd1*L1+gvd2*L2)/2           % average dispersion
FWHM = 3.125;
largo = FWHM/1.665;  %calculation of Gaussian pulse width
%%%%%%%%%%%%%%% pulse initialization %%%%%%%%%%%%%%
S = (L2*gvd2-L1*gvd1)/FWHM^2
E0=1;   % pulse energy in PJ
peako=sqrt(2/pi)*E0/largo;    % peak amplitude of Gaussian pulse
fmax=160/(2*pi*largo);    % maximum frequency
coef_dz=10.e-2;           % a fraction useful to set spatial steps
T0 = 800;           % temporal window
nt = 1000;           % Number of possible points
dt = 0.2;
%%%%%%%%%%%%%%%% initialization of time and frequency points
 df=1/T0;
fmax=1.0/(2.0*dt);
dw=2*pi*df;
wmax=2*pi*fmax;
%   Definition of temporal and frequency variables
 n1=nt/2;n2=n1-1; mil=n1+1;
t=(-n1:n2)*dt; h=dt;
w=(-n1:n2)*dw;
```

```
f=w/(2*pi);
u1=sqrt(peako).*exp(-t.^2/largo^2); % initial Gaussian pulse
UU = u1;
% nonlinear fiber lengths
L_NL1=1/(gamma1*peako);
L_NL2=1/(gamma2*peako);
L_D1=largo^2/abs(gvd1);       % anomalous dispersion length
L_D2=largo^2/abs(gvd2);       % normal dispersion length
 zstep1=coef_dz;
zstep2=coef_dz;
fmax=1/(2*dt);
 % calculation of spatial step sizes
npt1=2*round(0.5*L1/zstep1);
zstep1=L1/npt1;
npt2=round(L2/zstep2);
zstep2=L2/npt2;
 z=0;       % initial point of the fiber
li1=1;
zz(li1)=z;  %saving of spatial data
 U = u1;
for li2=1:1     % propagation for only one dispersion map
 % first-half of anomalous dispersion fiber
for indice=1:npt1/2
%%%% re-assinging new variables %%%%%%%%
beta2=gvd1;
gamma=gamma1;
dz=zstep1;
disper=exp(+i*beta2*dz*w.^2/2/2);
  % first 'half' dispersion calculation
V = fftshift(ifft(U));      % Fourier transform
V = V.*disper;          % calculation of dispersion
  U = fft(fftshift(V));       % Inverse Fourier transform
% 'full' nonlinearity calculation
P = abs(U);
```

```
P = P.^2;            % Intensity P
U = U.*exp(dz*(i*gamma*P));      % calculation of nonlinear
% second 'half' dispersion calculation
V = fftshift(ifft(U));       % Fourier transform
V = V.*disper;          % calculation of dispersion
  U = fft(fftshift(V));        % Inverse Fourier transform
z = z + dz;          % Incrementation of z
% saving data
if mod(indice,niter) == 0
 z
 li1=li1+1;
 UU =[UU; U];
 %saving the 'z' values where the fields are saved
zz(li1)=z;
end % for if
end % for indice
z
li1=li1+1;
UU =[UU; U];
%saving the 'z' values where the fields are saved
zz(li1)=z;
%full normal dispersion fiber
for indice=1:npt2
  %%%% re-assinging new variables %%%%%%%%
beta2=gvd2;
gamma=gamma2;
dz=zstep2;
 disper=exp(+i*beta2*dz*w.^2/2/2);
% first 'half' dispersion calculation
V = fftshift(ifft(U));       % Fourier transform
V = V.*disper;          % calculation of dispersion
U = fft(fftshift(V));        % Inverse Fourier transform
 % 'full' nonlinearity calculation
P = abs(U);
```

```
P = P.^2;            % Intensity P
U = U.*exp(dz*(i*gamma*P));      % calculation of nonlinear
% second 'half' dispersion calculation
  V = fftshift(ifft(U));       % Fourier transform
V = V.*disper;           % calculation of dispersion
U = fft(fftshift(V));        % Inverse Fourier transform
z = z + dz;          % Incrementation of z
% saving data
if mod(indice,niter) == 0
z
li1=li1+1;
%saving the field
UU =[UU; U];
%saving the 'z' values where the fields are saved
  zz(li1)=z;
  end % for if
 end % for indice
z
 li1=li1+1;
%saving the field
UU =[UU; U];
%saving the 'z' values where the fields are saved
zz(li1)=z;
%second-half of anomalous dispersion fiber
for indice=1:npt1/2
%%%% re-assinging new variables %%%%%%%%
beta2=gvd1;
gamma=gamma1;
dz=zstep1;
disper=exp(+i*beta2*dz*w.^2/2/2);
% first 'half' dispersion calculation
V = fftshift(ifft(U));       % Fourier transform
V = V.*disper;           % calculation of dispersion
U = fft(fftshift(V));        % Inverse Fourier transform
```

```
% 'full' nonlinearity calculation
  P = abs(U);
P = P.^2;            % Intensity P
U = U.*exp(dz*(i*gamma*P));      % calculation of nonlinear
% second 'half' dispersion calculation
V = fftshift(ifft(U));       % Fourier transform
  V = V.*disper;           % calculation of dispersion
  U = fft(fftshift(V));        % Inverse Fourier transform
z = z + dz;          % Incrementation of z
  % saving data
if mod(indice,niter) == 0
  z
li1=li1+1;
%saving the field
UU =[UU; U];
%saving the 'z' values where the fields are saved
zz(li1)=z;
end % for if
end % for indice
z
li1=li1+1;
%saving the field
UU =[UU; U];
%saving the 'z' values where the fields are saved
zz(li1)=z;
end % for li2
% 3D plot of the pulse
figure
waterfall(t,zz,abs(UU).^2);
title('SMF and DCF pulse propagation in one map period');
ylabel('z (km)');
zlabel('INTENSITY');
xlabel('t (ps)');
```